Calcium Chemistry as A New Member of Post-Lithium Battery Family: What Can We Learn from Sodium and Magnesium Systems

Zhenyou Li, Shuangshuang Cui, Joachim Häcker, Maryam Nojabaee, Maximilian Fichtner, Guanglei Cui,* and Zhirong Zhao-Karger**

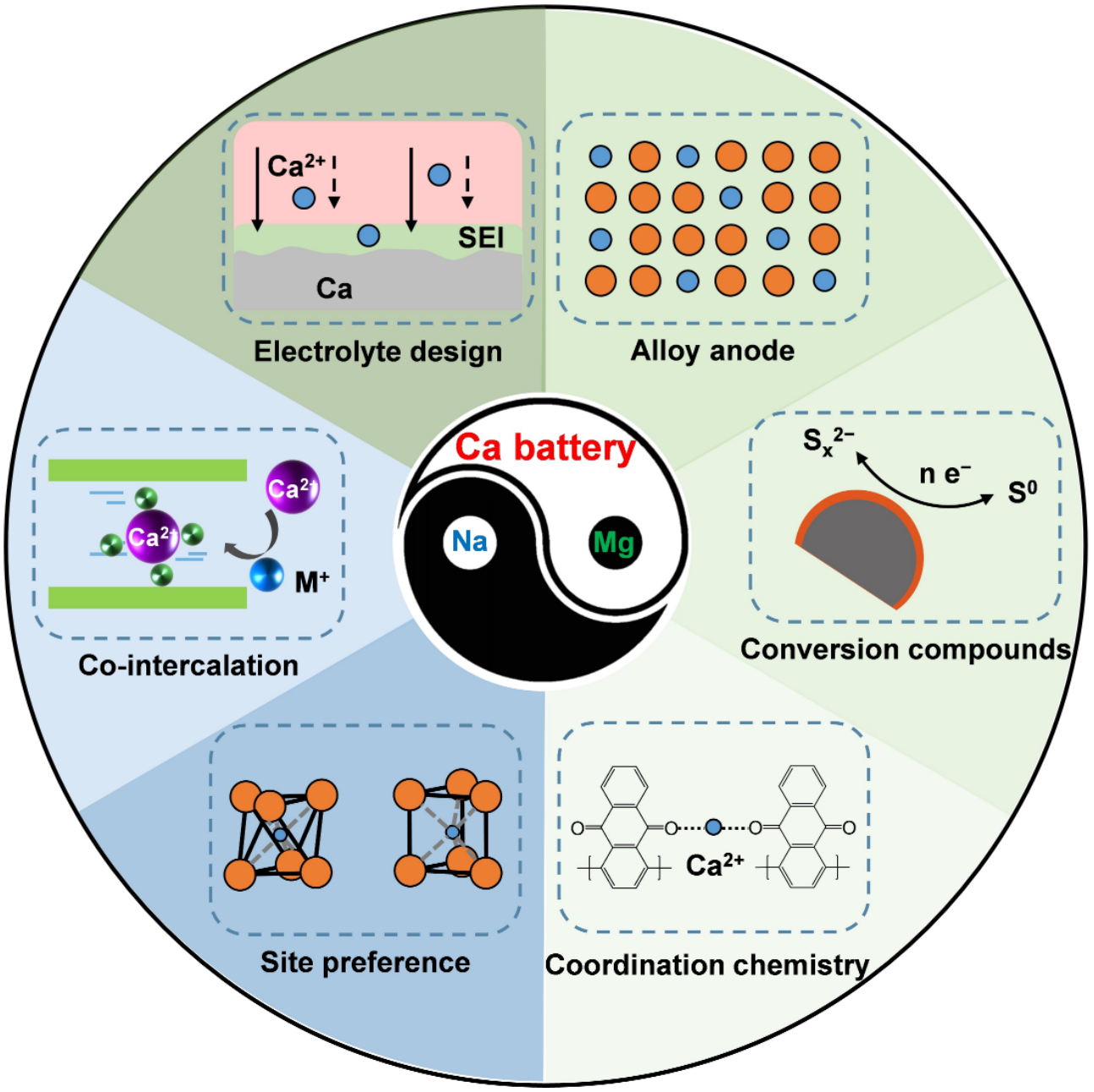

Abstract: The development of next-generation battery technologies needs to consider their environmental impact throughout the whole cycle life, which has brought new chemistries based on earth-abundant elements into the spotlight. Rechargeable calcium batteries are such an emerging technology, which shows the potential to provide high cell voltage and high energy density close to lithium-ion batteries. Additionally, the use of Ca^{2+} as a charge carrier renders significant sustainable values. Although pioneering work on the electrochemistry of Ca has been carried out for more than half a century, demonstration of reversible Ca^0/Ca^{2+} redox chemistry in non-aqueous media was only achieved within the past decade. In this review, we will present recent development of rechargeable calcium batteries, focusing on mainly the similarities but also differences between Ca chemistry and other post-lithium chemistry. According to the periodic nature of elements, magnesium (an alkaline earth element as Ca) and sodium (a diagonally adjacent element to Ca) have similar chemical properties to Ca in various aspects. We shall elaborate on how the solution chemistry, metal behaviors and transport mechanisms of Ca-ions can be better understood in light of the established principles in the respective Mg/Na systems. We hope the discussion will inspire synergetic development between Ca batteries and other post-lithium systems.

1. Introduction

Electrochemical energy storage (EES) technologies enable the use of renewable energy in a portable and reliable manner, playing an irreplaceable role in decarbonisation of electricity systems as well as e-mobility. Among others, lithium-ion battery (LIB) is the leading EES technology that has been widely deployed in e-vehicles and consumer electronics, and started to apply in the field of grid storage. Recently, the world leading battery manufacturer CATL launched a 500 $Wh\,kg^{-1}$ condensed matter battery, which opens the avenue towards e-aviation.[1] There is no doubt that LIBs will still dominant the battery market in the coming years, due to their superior storage performance. However, their reliance on critical raw materials such as cobalt, lithium (Li) etc. raise growing concerns on the long-term availability and sustainability of the technology.[2] The issue becomes more challenging as the EES market is expected to go through an exponential growth period in the coming decades.[3] This inspires research to shift toward chemistries that use more earth-abundant elements, leading to the development of so-called post-lithium batteries, such as sodium-ion batteries, rechargeable magnesium batteries etc.

In recent years, rechargeable calcium batteries (RCBs) emerged as a new member of the post-lithium family.[4] Calcium (Ca) is the fifth most abundant element in the Earth's crust, rich in living creatures, and has an even resource distribution worldwide. In addition to the resource advantage, the primary driving force to investigate RCBs is the low reduction potential of Ca^{2+}, which is only 0.17 V higher than that of Li^+ (Figure 1a). Hence, given the same cathode being employed, RCBs are capable of providing cell voltage close to LIBs. Furthermore, Ca metal anodes provide theoretical capacity of 2073 $mAh\,cm^{-3}$ volumetrically and 1337 $mAh\,g^{-1}$ gravimetrically, both of which are higher than sodium (Na), with the volumetric value similar

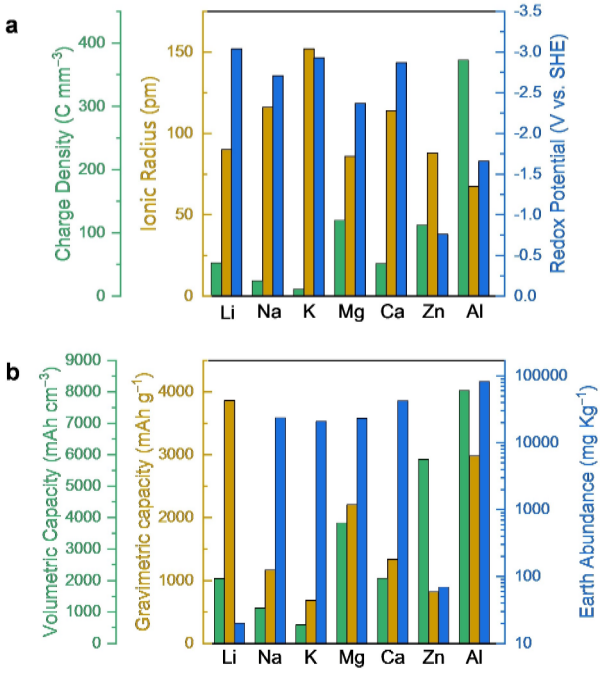

Figure 1. Comparison of (a) various metal cations in terms of charge density, ionic radius, and redox potential; and (b) the respective metals in terms of volumetric/gravimetric capacity and earth abundance.

[*] Prof. Z. Li,[+] Dr. S. Cui,[+] Prof. G. Cui
Qingdao New Energy Shandong Laboratory
Qingdao Institute of Bioenergy and Bioprocess Technology
Chinese Academy of Sciences
No. 189 Songling Road, Laoshan District, Qingdao, Shandong 266101, China
E-mail: lizhenyou@qibebt.ac.cn
cuigl@qibebt.ac.cn

Prof. Z. Li,[+] Prof. M. Fichtner, Dr. Z. Zhao-Karger
Helmholtz Institute Ulm (HIU) Electrochemical Energy Storage
Helmholtzstraße 11, D-89081 Ulm, Germany
E-mail: zhirong.zhao-karger@kit.edu

Dr. J. Häcker, Dr. M. Nojabaee
Institute of Engineering Thermodynamics
German Aerospace Center (DLR)
Pfaffenwaldring 38–40, 70569 Stuttgart, Germany

Prof. M. Fichtner, Dr. Z. Zhao-Karger
Institute of Nanotechnology (INT)
Karlsruhe Institute of Technology (KIT)
P.O. Box 3640, D-76021 Karlsruhe, Germany

to Li (Figure 1b). As a charge carrier, Ca^{2+} should in principle have the best diffusion kinetics among the multivalent cations. Due to the larger ionic radius, the charge density of Ca^{2+} is similar to that of Li^{+}, and ~40 % the value of Mg^{2+}.[5] All these merits make RCB a promising next-generation storage technology for large-scale grid applications as well as for surface vehicles, featuring sustainability, cost-effectiveness, and high-energy, provided that the rate capability can be enhanced.

First attempt to implement Ca as an electrochemical active element in a battery date back to the 1960s, targeting the primary thermal batteries.[6] However, the pioneering work investigating the electrochemical behaviour of Ca metal anodes in non-aqueous electrolytes was reported in the 1990s, when Aurbach et al. found severe passivation of Ca in aprotic solvents and conventional Ca electrolyte compounds.[7] In 2016, Ponrouch et al. demonstrated the feasibility of reversible Ca plating/stripping from carbonate-based electrolytes at moderate operating temperature, which re-captures the research interest in exploring viable materials for Ca-based batteries.[8] Starting from 2018, there were significant progresses in the development of Ca batteries, which was initiated by the development of Ca electrolytes, particularly calcium borohydride in tetrahydrofuran $Ca(BH_4)_2$/THF[9] and calcium tetrakis(hexafluoroisopropyloxy)borate in dimethoxymethane $Ca[B(hfip)_4]_2$/DME,[10] which allow electrochemical plating/stripping of Ca at room temperature with high efficiency. The advancement in electrolytes triggered intensive investigation of the electrode materials. This resulted in two representative anode materials, i.e. graphite[11] and calcium-tin (Ca–Sn) alloys,[12] both of which provide significantly enhanced anode-electrolyte interfaces for long-term cycling. On the cathode side, polyanion structures, such as Olivine iron phosphate ($FePO_4$) and the natrium super ionic conductor (NASICON) compounds,[13] were discovered capable of accommodating Ca^{2+} at high voltages. Bringing all these progresses together might lead to benchmark Ca-based batteries in the near future that would further accelerate the development of RCB technology.

Despite that, RCBs is still in an early stage of R&D. The battery performance is still far behind the commercially available storage technologies.[4a,14] The grand challenge that hinders the development of RCBs is the generally low reversibility of Ca-based electrochemistry. This is particularly the case for plating/stripping of Ca at the anode side. As metallic Ca is highly reactive, it easily forms surface passivating film in organic electrolyte that impedes further redox reactions.[7] In addition, divalent Ca^{2+} prefers a high coordination number with certain flexibility, which gives rise to a rather complex solvation structure of Ca^{2+} in electrolytes and complicated interfacial processes with high kinetic barriers.[15] Kinetic issues are also encountered for Ca^{2+} storage in the cathode. In spite of a fairly low charge density, Ca^{2+} diffusion in conventional transition metal compounds still suffers from high energy barrier,[16] probably due to its large ionic radius plus bivalency. Worse is that, the size effect may lead to strong repulsion between the neighbouring intercalants in the cathode lattice, inducing detrimental

phase transition that hinders the reversibility of Ca^{2+} insertion, similar to the case of Na^+ storage.[17]

In this review, we would like to systematically evaluate the chemistries in rechargeable Ca battery from the perspective of other more mature battery chemistries. As Ca battery is an emerging battery technology, such a comparative evaluation would greatly accelerate the developing process by avoiding unnecessary trial and error, and allowing transfer of knowledge directly from other battery systems. Ca is an alkaline earth element following magnesium (Mg) in the periodic table (Figure 2), therefore sharing similar chemical and electrochemical properties to Mg. Particularly the solution chemistry and metal/alloy behaviors of Mg would provide valuable insights for the design of viable Ca electrolyte as well as stable anode interface/interphase. The similarity also goes for organic redox chemistry (coordination chemistry) and conversion chemistry between Mg and Ca, due to their bivalency. Similarly, zinc (Zn) is also a divalent metal. However, most research on rechargeable Zn batteries employs aqueous electrolytes. As water (H_2O) has strong solvation power, the redox chemistries differ from those in non-aqueous solutions. As a result, a comparison between Zn and Ca chemistries will not be the focus of this review. On the other hand, when it comes to ion mobility and storage within the rigid crystal lattice, the size effect is playing a more critical role. In layered compounds, large intercalants (Na^+, K^+, Ca^{2+}) prefer P3 stacking sequence to minimize electrostatic repulsion, while small intercalants (Li^+, Mg^{2+}) prefer O1 or O3 stacking.[17] As the ionic radius of Ca^{2+} (1.14 Å) is close to Na^+ (1.16 Å), the site preference, migration pathways and phase stability of Ca^{2+}-based insertion chemistry could learn from the respective sodium (Na) system. Considering the generally fast kinetics of Na^+-based insertion chemistry, this similarity gives a great hope to the community for enabling fast-charging Ca cathode. Overall, we expect the review to provide fundamental understanding of the charge storage mechanisms and the migration behavior of Ca-ion, hoping to sparkle more diverse ideas for the exploration of tailor-made materials for RCBs.

2. Electrolyte Design

Metallic Ca has been identified as a promising anode material for high-energy batteries beyond Li, by providing a high theoretical capacity but also a low redox potential close to that of Li. In search for electrolyte that is compatible with Ca metal anode, pioneering efforts were made to screening conventional Ca compounds whose Li analogues were already applied in Li-based batteries. However, these electrolytes readily react with Ca, forming surface passivation layer that impedes further electrochemical reactions. Note, surface passivation was a similar issue facing Mg chemistry. Taking into account that Mg and Ca being both alkaline earth elements, further attempts were made to transfer the knowledge established in Mg electrolyte to the design of Ca electrolyte. This has led to the development of calcium borohydride as the first electrolyte allowing reversible plating/stripping of Ca at room temperature, but also viable Ca electrolytes based on weakly coordinating anions.

In this section, we would like to start with a comparison of physicochemical properties between Ca and Mg, in both elemental state and ionic form. This is followed by elaborating how the similarities enable knowledge transfer from Mg to Ca system and the discovery of functioning Ca electrolytes. Particularly, their solvation structure will be elucidated, highlighting how the solvents and additives are affecting the solvation structure, bulk ionic transport and interfacial properties. In addition, we will point out intrinsic difference between Ca^{2+} and Mg^{2+} in terms of coordination number in solution, ion mobility within interphases etc., as previously overlooked challenges.

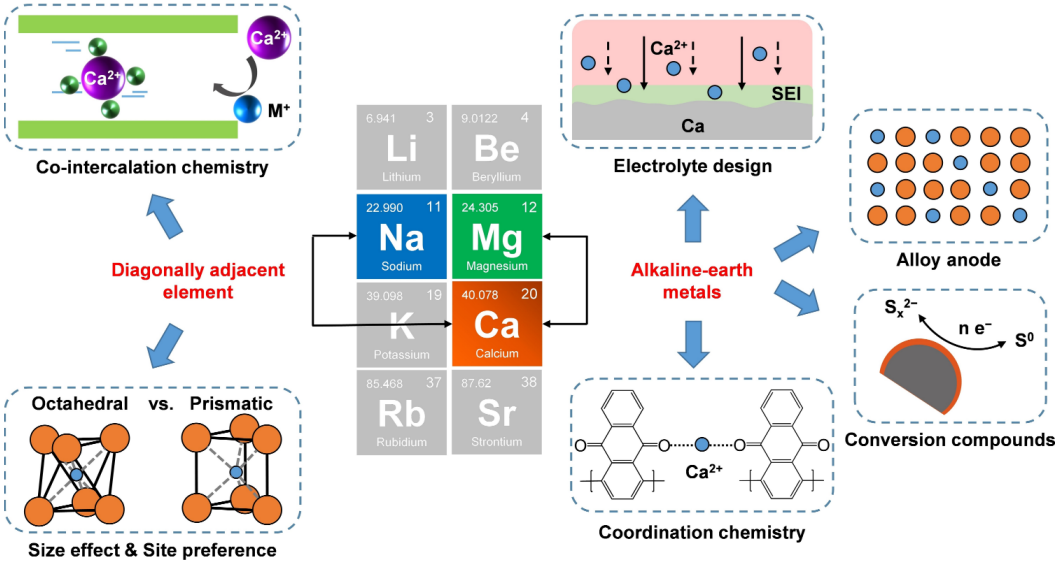

Figure 2. Scope and overview of the content discussed in this review.

Ca exhibits a lower redox potential of −2.87 V vs. SHE which is close to that of Li (−3.04 V vs. SHE) and 0.5 V lower than that of Mg (−2.37 V vs. SHE). In addition, Ca^{2+} ion exhibits a larger radius (1.00 Å) than Mg^{2+} ion (0.72 Å) while carrying the same charge.[18] The low charge to size ratio of Ca^{2+} results in a charge density of Ca^{2+} (52 C mm^{-3}), which is close to that of Li^+ and less than half of that of divalent ions Mg^{2+} (120 C mm^{-3}) while Na^+ has an even lower value of 24 C mm^{-3}. The softness of Ca^{2+} ions induces a low polarizability and weak interaction with surrounding coordination environment, which may potentially enable fast Ca^{2+} ion transport and diffusion in electrolytes and host materials. However, incompatibility of Ca metal with the common electrolyte salts and solvents poses the challenges in the development of suitable electrolytes for Ca batteries.

2.1. Ca Electrolytes in Carbonates

Early studies on Ca-ion electrolytes were conducted in the electrolytes analogous to those used lithium-ion batteries (LIBs). The first reversible Ca deposition was demonstrated by Ponrouch et al. on stainless steel using calcium tetrafluoroborate ($Ca(BF_4)_2$) in carbonate solvents at elevated temperatures (75–100 °C) as shown in Figure 3a.[8] A considerable amount of CaF_2 was observed on the Ca electrode, indicating high interfacial reactivity of Ca metal. The Ca^{2+} solvation chemistry in carbonates has been revealed to be unique among alkali and alkaline earth cations. Due to its large ionic radius and bivalency, Ca^{2+} has the highest coordination number of solvating molecules in carbonates (6–9, typically ~8) compared to Li^+, Na^+, and Mg^{2+} (4, 4, and 5, respectively), as determined by MD simulations.[19] In addition, solvation free energies, determined by density functional quantum chemical calculations for different Ca^{2+} solvation structures, ranged from −385 to −472 kcal mol^{-1}, substantially more negative than those of Na^+, Li^+, and even Mg^{2+} (−215 to −329 kcal mol^{-1}) as depicted in Figure 3b.[20]

While higher solvation energies increase the solubility of the electrolyte salts, they also create a trade-off by introducing high desolvation energy barriers for Ca plating. This may partly contribute to the need of high temperatures for reversible Ca deposition using carbonate electrolytes, in addition to the energy barriers for ion pair dissociation and at the Ca metal interfaces.

2.2. $Ca(BH_4)_2$ in Ether Solvents

The first room-temperature Ca electrolytes was reported by Wang et al. using the solution of $Ca(BH_4)_2$ in THF solution (Figure 4a). Beneficial from its inherent reducibility, the use of $Ca(BH_4)_2$ can prevent the surface passivation of Ca surface, enabling the reversible electrochemical Ca plating/stripping with up to 94 % Coulombic efficiency.[21] Moreover, the formation of CaH_2 was revealed, which most likely originate from the borohydride rather than the reaction between Ca and THF.[22] It is worth mentioning that $Ca(BH_4)_2$, as a reducing agent, has the limitations in terms of relatively low electrochemical stability (< 3 V) and chemical incompatibility with certain cathode materials such as sulfur.[23]

Jie et al. further studied the interplay between solvation energy, interfacial reactions and electrochemical performance.[24] To decrease the coordination number of Ca^{2+} and reduce the solvation energy, $LiBH_4$ was blended into the $Ca(BH_4)_2$/THF electrolytes. It was revealed that the addition of $LiBH_4$ led to the formation of spherical deposits composed of Ca, $CaCO_3$, CaO, and THF decomposition products, which was proven to be beneficial for enhancing reversible Ca deposition. Another investigation of the SEI formation in $Ca(BH_4)_2$/THF electrolytes with additional approximately 0.004 M $NaBH_4$ was conducted using cryogenic TEM analysis. It demonstrated the formation of dense Ca deposits and the interphase composed of nanometric calcium oxide structure, with a small fraction of calcium borate and calcium carbonate species.[25]

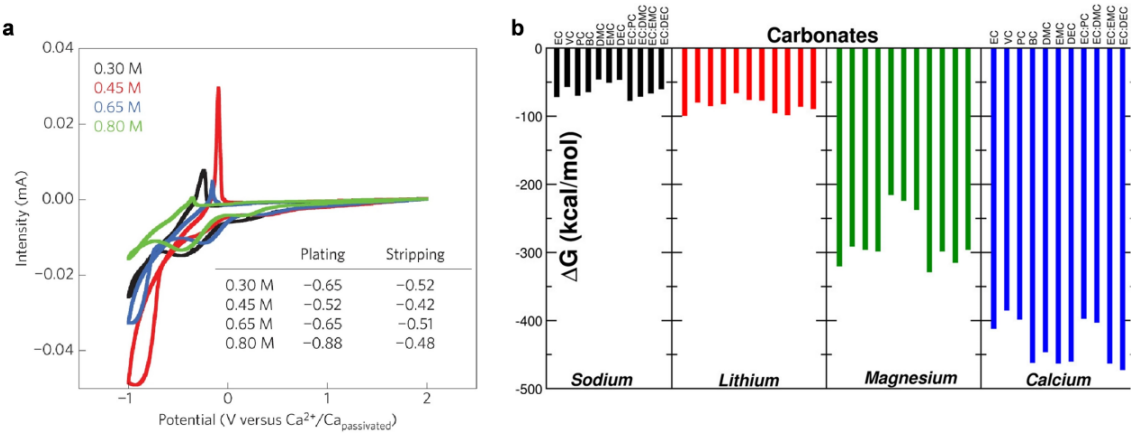

Figure 3. (a) CVs showing Ca plating/stripping with $Ca(BF_4)_2$ in EC:PC solutions at 100 °C and 0.5 mV s^{-1}. Reproduced with permission.[8] Copyright 2016, Springer Nature. (b) Solvation free energy of Li^+, Na^+, Mg^{2+}, and Ca^{2+} in carbonates. Reproduced with permission.[20] Copyright 2019, American Chemical Society.

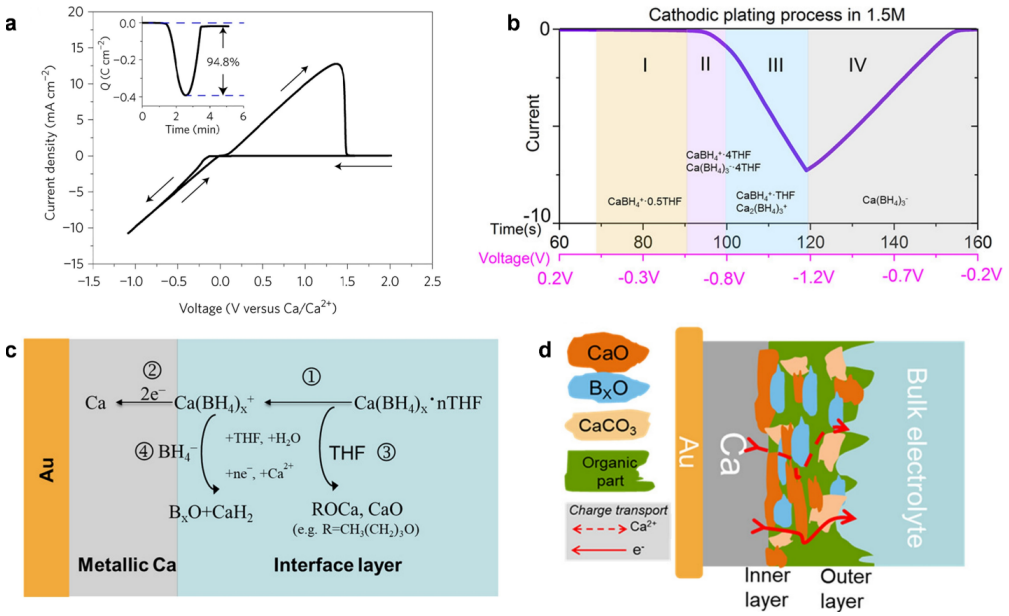

Figure 4. (a) CV showing Ca plating/stripping with $Ca(BH_4)_2$ in THF on Au working electrode at room temperature. Reproduced with permission.[9] Copyright 2018, Springer Nature. (b) Proposed key surface intermediates identified by EQCM-D data on the Au surface in the 1.5 M electrolyte cell during the first cathodic plating process as a function of time (corresponding potential scale is shown in magenta, and (c) Scheme of the proposed surface electrochemical reaction pathways during the first Ca electrodeposition process for 1.5 M electrolyte. (d) Schematic illustration of the SEI layer formed on the plated Ca electrode in 1.5 M $Ca(BH_4)_2$/THF electrolyte. Reproduced with permission.[26] Copyright 2023, American Chemical Society.

Recently, the coordination and solvation structures of $Ca(BH_4)_2$/THF electrolytes were investigated using electrochemical quartz crystal microbalance with dissipation (EQCM-D).[26] The process of Ca deposition was unveiled to be more intricate than a straightforward two-electron mechanism, involving the compositional transformation of the cation-anion complexes within their solvation shells, such as $CaBH_4^+ \cdot 4THF$ or $Ca(BH_4)_3^- \cdot 4THF$, and finally the desolvation step (Figure 4b). Figure 4c illustrates the possible reaction pathways for Ca deposition process in $Ca(BH_4)_2$/THF electrolytes. The components of the SEI layer were identified through XPS, as depicted in Figure 4d. These components include calcium oxide, borates, carbonate and some organic species, which align with previous reports.[24]

2.3. Ca Conductive Salts with Stable and Weakly Coordinating Anions

In 2019, two independent studies demonstrated that the $Ca[B(hfip)_4]_2$ salt exhibits promising electrolytic properties,[10] where we synthesized the salt via a straightforward route by reacting $Ca(BH_4)_2$ with hexafluorisopropanol (hfip-H) in DME while Shyamsunder et al. carried out an alternative two-step synthesis with $Ca(hfip)_2$ and $B(hfip)_3$. The salt is analogous to the successful $Mg[B(hfip)_4]_2$ electrolyte.[27] The highly delocalized electronic structure of the bulky hfip anion may lead to weak interaction with the cation, allowing reversible Mg/Ca plating/stripping at room temperature. The 0.25 M $Ca[B(hfip)_4]_2$ in DME exhibited an ionic conductivity of 8.3 mS cm^{-1}, oxidative stability of >4 V vs. Al or stainless steel, and a high peak current of ~20 mA cm^{-2} for plating/stripping and a Coulombic efficiency of ~80 % in the CV (Pt working electrode, 80 mV s^{-1}, Figure 5a).[10a] A moderate CaF_2 content (~7 %) on the Ca deposits was observed, which was attributed to the chemical reduction of the anions. A recent study using cryo-electron microscopy (cryo-EM) to investigate calcium deposition in $Ca[B(hfip)_4]_2$/DME electrolytes revealed that the calcium deposits form spherical structures covered by amorphous layers comprised of CaF_2, CaO, $CaCO_3$ as shown in Figure 5c.[28] Additionally, a high migration energy barrier of approximately 2046 meV was calculated for CaF_2,[29] suggesting that Ca^{2+} ion transport could be restricted by the surface layer formed in the electrolytes.

Moreover, solvation effects of metal ions significantly impact the performance of the electrolytes by influencing ionic conductivity, stability, transport properties, and electrode interactions. Based on the single crystal X-ray diffraction analysis of the as-prepared $Ca[B(hfip)_4]_2$ salt, Ca^{2+} was found to be coordinated by 4 DME molecules in the crystal structure (Figure 5b), in which the average O–Ca bond length (2.43 Å) of the DME-coordinated Ca^{2+} is longer than that of Mg^{2+} in the analogous crystal (2.06 Å). It was suggested that the desolvation energy of Ca^{2+} might be slightly lower than that of Mg^{2+} in solution, which aligns with its relatively lower charge density. On the other hand, Ca^{2+}, with a larger ionic radius of 1.00 Å, adopts a different coordination geometry in $Ca[B(hfip)_4]_2 \cdot 4DME$ and has a higher coordination number (CN) of 8, in contrast to the analogous Mg salt,[27] which coordinates with 3 DME molecules with a CN of 6. Understanding the influence of

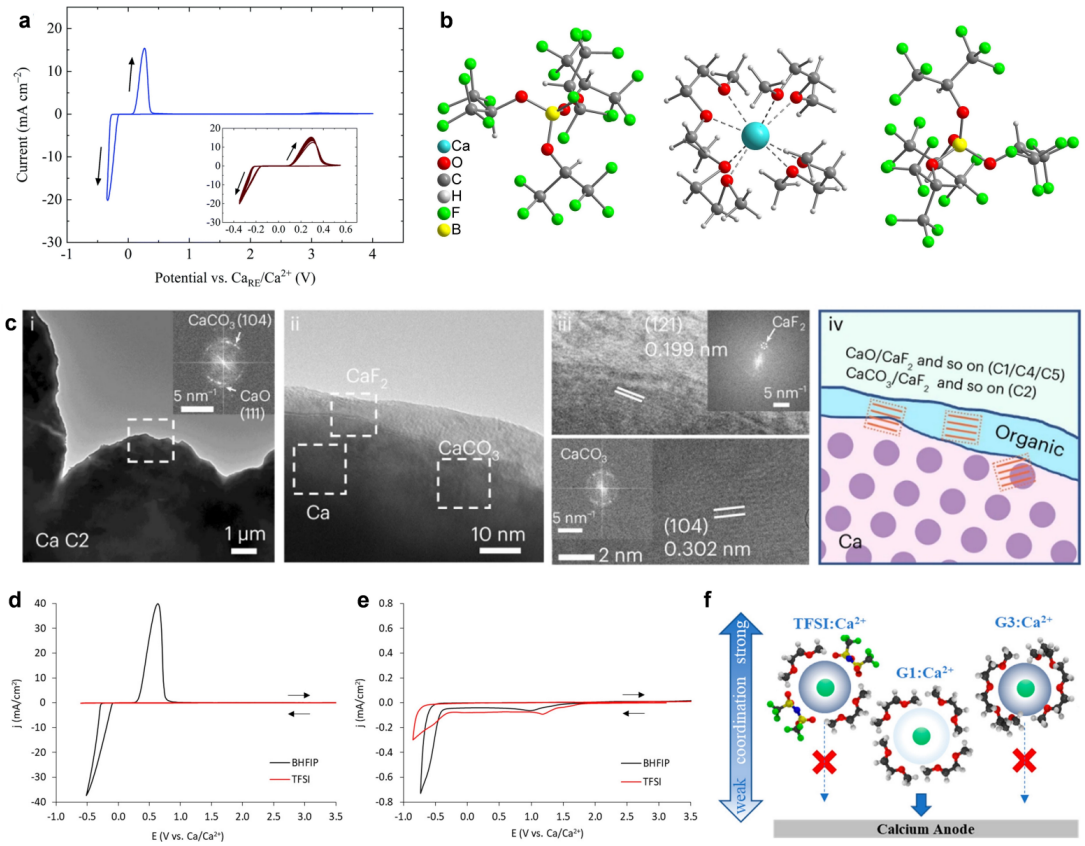

Figure 5. (a) CV showing Ca plating/stripping of Ca[B(hfip)$_4$]$_2$/DME electrolytes on Pt at room temperature and 80 mV s^{-1}. (b) Single crystal structure of Ca[B(hfip)$_4$]$_2$. Reproduced with permission.[10a] Copyright 2019, Royal Society of Chemistry. (c) Cryo-EM images of Ca deposits and surface layer in Ca[B(hfip)$_4$]$_2$/DME electrolytes Reproduced with permission.[28] Copyright 2024, Springer Nature. CV showing Ca plating/stripping in Ca(TFSI)$_2$ and Ca[B(hfip)$_4$]$_2$ in (d) G1 and (e) G3, (f) Illustration of the influence of anion and solvent coordination strength on Ca^{2+} reduction. Reproduced with permission.[30a] Copyright 2020, American Chemical Society.

solvation structure and coordination strength on the electrolyte properties, including solubility, transport, and electrochemical stability, is essential for optimizing electrolyte compositions. Hahn et al. reported their studies combined spectroscopic analysis with MD simulations to characterize ion association tendencies of Ca(TFSI)$_2$ and Ca[B(hfip)$_4$]$_2$ in ethereal solutions.[30] A clear trend in coordination strength between Ca^{2+} and the solvent has been demonstrated as 2-MeTHF < THF < DME (G1) < diglyme (G2) < triglyme (G3). Moreover, the differences in anion coordination strength and the influence of these anions on coordination structures have been investigated. As shown in Figure 5d, Ca(TFSI)$_2$ is not capable of Ca plating/stripping in these ethereal solutions due to the prevalent Ca^{2+}-$TFSI^-$ contact ion pairs in the relatively weaker solvating solvents (such as THF, G1) or anion dependent solvation structures in strongly solvating solvents like G2 and G3. In contrast, weakly coordinating anion $[B(hfip)_4]^-$ facilitate ion dissociation in G1, allowing reversible Ca deposition and stripping in agreement with previous reports. Interestingly, it was revealed that the use of a strongly coordinating ethereal solvent such as G3 may inhibit Ca deposition in Ca[B(hfip)$_4$]$_2$ solutions due to the high desolvation energy needed for the plating process. Recently, another DFT study unveiled that in short chain glymes such as DME, the transferred electron is located on a Ca^{2+} center and the organic part of the solvation sphere, benefiting for the Ca^{2+} reduction. As the glyme's length increases to tetraglyme (G4), a greater activation energy is required for desolvation, which may induce a large overpotential and degradation of the electrolyte components.[31]

Further, a study by Nilson et al. investigated the Ca[B(hfip)$_4$]$_2$ electrolytes in different ethereal solvents,[32] demonstrating the diglyme solution exhibited superior electrochemical performance in terms of the lowest polarization and longest cycling stability in symmetric cells. Additionally, the Ca deposits appeared predominantly smooth dendrite-free morphology. These properties might be attributed to the favorable solvent effects.

Due to the chemical similarity between B and Al, researchers have also explored alkoxyaluminate-based electrolytes for Ca batteries through both computational and experimental studies.[33] Recently, the investigation of the calcium tetrakis(hexafluoroisopropyloxy) aluminate salt, Ca[Al(hfip)$_4$]$_2$, was reported, further confirming the feasibility of this salt for the use as a Ca electrolyte.[33b] This salt exhibited comparable electrochemical performance to Ca[B(hfip)$_4$]$_2$ electrolytes in terms of oxidative stability and ionic

conductivity. However, the synthesis of $Ca[Al(hfip)_4]_2$, similar to its Mg analog, depends on the use of the highly moisture-sensitive organoaluminium compound such as $Al(CH_3)_3$. The need for stringent conditions can lead to high synthetic costs and would be a major drawback from the application point of view. In addition, CaF_2 formation on Ca deposits in aluminate electrolytes was also observed.

In 2021, a fluorine-free Ca electrolyte, utilizing calcium monocarborane ($Ca(CB_{11}H_{12})_2$) in a binary mixture of THF and DME, was reported.[34] Featuring a weakly coordinating hydrogen cluster, this electrolyte demonstrated a wide electrochemical potential window of up to 4 V against Au and a high ionic conductivity at 4 mS cm^{-1}. Additionally, it enabled reversible Ca metal plating and stripping at room temperature with a Coulombic efficiency of approximately 88 %. The Ca deposits on the Au electrode was characterized by XRD and SEM, revealing the prevalence of Ca metal, along with a small amount of CaH_2 and electrolyte decomposition products composed of Ca, O, C and B. This electrolyte has been reported to be compatible with various cathode materials, such as sulfur and copper sulfide.[35] Despite the favorable electrochemical properties and good Ca anode compatibility of F-free carborane electrolytes, the nontrivial synthesis, and the associated high costs may restrict its practical application.

In addition to the design of new Ca electrolytes, strategies were also explored to enable Ca plating/stripping in commercial Ca compounds with weakly coordinating anions, such as $Ca(TFSI)_2$ and $Ca(BF_4)_2$. As mentioned before, these Ca compounds were found to passivate Ca metal anode at room temperature. However, recent studies demonstrated the feasibility to enhance their compatibility with Ca metal anode by tailoring the solid-electrolyte interphases (SEIs). Ponrouch et al. carried out a comprehensive investigation on the plating deposits from $Ca(BF_4)_2$ in EC/PC, and revealed organic borates derived from BF_4^- as a key SEI component.[29] This approach was further extended by introducing BF_3 complex as electrolyte additive that resulted in a similar SEI on the Ca anode and promoting Ca deposition in a $Ca(TFSI)_2$/EC-PC electrolyte.[36] More generally, these studies suggest eliminating inorganic components in SEI layers that create significantly high migration barriers for Ca^{2+}.[29] To minimize the anion-derived inorganic-rich SEIs, Zhang et al. employed strong solvating solvent dimethylacetamide to promote dissociation of $Ca(TFSI)_2$, leading to the formation of an organic-rich, CaF_2-poor SEI that allowed stable cycling of Ca metal anode for 100 h.[37] On the other hand, CaH_2 was predicted to have the lowest migration barrier of 541 meV among all the investigated inorganic SEI components.[29] The result was in line with previous experimental study on the $Ca(BH_4)_2$/THF electrolyte, where CaH_2 was identified as a main SEI component.[9] In a very recent study, CaH_2 was even found in the deposits from the $Ca[B(hfip)_4]_2$/DME electrolyte.[38] Via chemical reactions between Ca metal anode and the $Ca[B(hfip)_4]_2$/DME electrolyte, CaH_2 as well as CaO and borate species were gradually formed upon aging. Note, metal hydrides are also effective SEI components in other battery systems including Li/Na/Mg batteries.[39] This suggests that the strategies promoting metal hydride formation in other battery chemistries might be applicable for building a CaH_2-based SEI in Ca batteries.

Overall, the inherent chemical properties of Ca^{2+} cations in organic solutions, coupled with the complex interfacial chemistry of Ca metal anodes, present significant challenges in developing calcium electrolytes. Recent progress has brought promising Ca electrolyte systems to the forefront, establishing new platforms for calcium battery research. While considerable effort has been devoted in understanding ion-pairing and solvation structures in the most successful electrolytes identified to date, further investigation is needed to clarify the confounding factors related to the composition, structure, and properties of the electrode-electrolyte interface and their impacts on Ca^{2+}/Ca redox processes. A deeper understanding of the unique chemistry of Ca^{2+} in electrolyte solutions and within the SEIs on Ca anodes is essential for future advancements.[40]

3. Alloy Anode

Despite significant progress made during the past years, the implementation of Ca metal anodes is still problematic. Even the state-of-the-art electrolytes suffer from decomposition during Ca plating/stripping, which resulted in limited cycle life and low area capacity (<1 mAh cm^{-2}).[41] In fact, the inhomogeneous reactions at the metal surface would induce effectively high current density at specific active area that might trigger detrimental dendrite growth.[42] The interfacial issue at the anode further affected the charge transfer at the cathode side, which makes the screening of cathode materials against metal anode still infeasible. Beside electrolyte design and interfacial engineering, employing alloy anodes with enhanced anode-electrolyte compatibility is an alternative approach.

Alloy anodes generally offer high capacity by triggering multi-electron alloying reactions, but also serve as Ca reservoir allowing the coupling with Ca-free cathode materials. As shown in Figure 6a, replacing Ca metal anodes by Ca-rich alloy anodes lead to only around 20 % reduction of the energy density in full-cells, given a hypothetic cathode with 200 mAh g^{-1} capacity and 3 V vs Ca/Ca^{2+} voltage is applied. Among others, Ca–Si and Ca–Sn were the first systems that were experimentally evaluated, due to the high-capacity, resource abundance and environmentally friendliness of Si and Sn. Ponrouch et al. demonstrated that decalciation of $CaSi_2$ was feasible, but suffered from sluggish reaction kinetics. This resulted in a quite limited reversibility of the process even at 100 °C.[43] The kinetics of de-/alloying process seemed to be better in case of the Ca–Sn system. By using a calciated Sn anode, Lipson et al. was able to cycle a Ca-ion battery with a manganese hexacyanoferrate cathode for more than 35 cycles at ambient temperature.[44] A capacity retention of ~50 % was obtained afterwards, likely due to the degradation of the Sn anode, which led to the loss of Ca reservoir at the anode. To further enhance the cyclability of Sn anode, a dual-ion batteries was proposed coupling Ca–Sn alloying reaction with anion intercalation

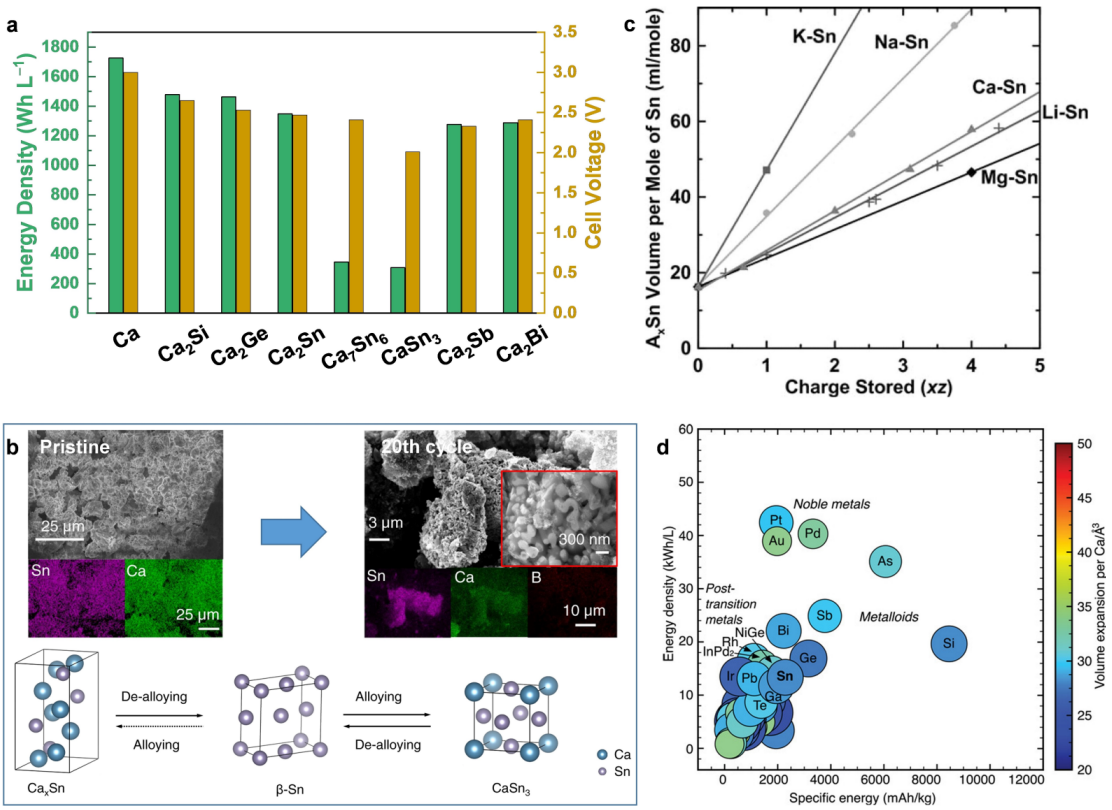

Figure 6. (a) A comparison of Ca metal anode with selected alloy anodes. The energy density and cell voltage are calculated based on a hypothetic cathode that provides 200 mAh g^{-1} capacity at voltage of 3.0 V vs Ca. (b) A comparison of different A_xSn alloys (A = Li, Na, K, Mg, Ca), in terms of volume per mole of Sn with respect to charge stored. Reproduced with permission.[12b] Copyright 2022, the Authors, published by Springer Nature. (c) Structural change of the Ca_xSn alloy (x ~2) over cycling. Reproduced with permission.[50] Copyright 2011, The Electrochemical Society. (d) Theoretical prediction of alloy anodes for Ca storage. Reproduced with permission.[45] Copyright 2019, Wiley.

into graphite as cathode reaction.[12a] The dual-ion cell configuration made use of electrolyte as Ca^{2+} reservoir, allowing long-term cycling of the Sn anode on the condition that flooded electrolyte is applied. As a result, the Ca-based graphite-Sn cells exhibited 95 % capacity retention after 350 cycles and provided a high cell voltage of close to 4.5 V. Further mechanistic investigation revealed the formation of Ca_7Sn_6 on the Sn anode, delivering a theoretical capacity of 526 mAh g^{-1} with a volume expansion of 136.8 %.[12a]

The breakthroughs of applying Sn anode for Ca-based batteries inspired further research activities to develop Ca–Sn alloy anodes. The shift from metallic Sn anode to Ca–Sn alloy anode also enabled the screening and evaluation of Ca-free cathode hosts. Based on the Ca–Sn phase diagram, Ca_2Sn has the highest Ca content among Ca–Sn alloys, therefore providing the highest capacity (903 mAh g^{-1} based on Sn) and the lowest redox potential (0.53 V vs. Ca).[45] Zhao-Karger et al. recently reported the synthesis of a Ca-rich $CaSn_x$ alloy and identified Ca_2Sn as the main phase.[12b] By employing the $CaSn_x$ alloy anode, a 1,4-polyanthraquinone (14PAQ) cathode was able to reversibly host Ca^{2+} for more than 5000 cycles at 260 mA g^{-1}, retaining a capacity of 78 mAh g^{-1}. On the contrary, the 14PAQ-Ca cell showed early cell failure after only 6 cycles. It was found that the $CaSn_x$ alloy underwent activation cycles leading to the formation of $CaSn_3$, which served as redox-active species in the subsequent cycling (Figure 6b). Compared to the chemically synthesized microsized $CaSn_3$, the electrochemically in situ formed $CaSn_3$ had a porous nanostructure, which gave rise to an enhanced kinetics and therefore high reversibility of the anode reactions. In fact, the alloying process from metallic Sn to $CaSn_3$ has a volume expansion of only 7.3 %,[45] which is beneficial for long-term cycling. The synthesized $CaSn_3$ was therefore further applied for the investigation of a polytriphenylamine (PTPAn) cathode in the $Ca[B(hfip)_4]_2$/DME electrolyte. The PTPAn cathode underwent redox of the amine functional groups during charge and discharge, thereby hosting $[B(hfip)_4]^-$ anions instead of Ca^{2+}. The PTPAn-$CaSn_3$ dual-ion batteries were cycled for more than 3000 cycles, with a capacity retention of ~60 %.[46]

Although the Ca–Sn alloys enabled significantly improved cycling stability of Ca-ion batteries, their maximum capacity that could be achieved experimentally was < 120 mAh g^{-1}, which was only 13 % of the theoretical value (903 mAh g^{-1} for Ca_2Sn), and with rather limited reversibility.[12b] This raised concerns on the kinetic issues of the de-/alloying processes, and calls for further comprehensive understanding of the reaction mechanism. The kinetic issue might be related to the sluggish diffusion of Ca atom

within the lattice of the Ca–Sn alloys. A similar issue was also encountered in Mg system, where neighboring Mg atoms tends to agglomerate and forms Mg–Mg complexes in the tetragonal Sn structure, leading to an increase of the migration barrier from 0.43 to 0.77 eV.[47] As a result, Mg atoms are more easily anchored on the surface of Sn rather than diffuse inside.[48] The sluggish diffusion kinetics of alkaline earth metals could also generate considerable mechanical stress, which possibly lead to unique reaction pathways different from the insertion of alkali metals.[49]

Another key factor that governs the de-/alloying process is the volume change. According to Vegard's law, the volume of an alloy A_xM (A = Li, Na, Mg, Ca etc.) per host metal atom M per unit charge stored in the alloy can be described by $V = xzk_A + v_0$, where V is the molar volume of the alloy per metal M, k_A is the volume occupied per unit charge stored in the alloy, and v_0 is the molar volume of pure metal M. Although Ca atom is large in size, it enables two charge transfer per atom. As a result, Ca_xSn alloys exhibit a volume expansion similar to the Mg_xSn and Li_xSn, and significantly lower than the Na_xSn alloys (Figure 6c).[50] As revealed by the same study, the trend of volume expansion can be generalized among various host metals, as each stored metal A has a characteristic volume in alloys. Nevertheless, volume expansion of Sn to form Ca_2Sn is still significant (183 %), which leads to pulverization of the active materials and degradation of the anode. As volume expansion is a general issue of alloy anodes, feasible strategies developed in other battery systems could be considered, such as particle downsizing, dispersing active alloy particles within a composite matrix, applying functional binder etc.[51]

Beyond Ca–Si and Ca–Sn alloys, there are plenty of alloying systems showing theoretically promising features, which leaves large room for the development of high-performance alloy anodes for calcium batteries. As predicted by a high-throughput computational analysis shown in Figure 6d, a large range of elements including metalloids, transition metals and noble metals, form alloy compounds with Ca at low voltages.[45] Particularly, some p block metals or the related alloy compounds already exhibited excellent performance in Mg-based battery systems, therefore deserve further investigation.[52]

4. Co-Intercalation Chemistry

Intercalation chemistry lays the foundation for the current commercially available Li-ion battery technology.[53] The robust host structures allow de-/intercalation of mobile Li^+ with high reversibility, thereby enabling long cycle life. The excellent performance of the intercalation compounds in LIBs also inspires investigation and evaluation on their capability to host Ca^{2+}. However, most of the intercalation compounds developed so far showed inferior cycling stability and rate capability compared to their Li analogues. Despite its lowest charge density among multivalent charge carriers, Ca^{2+} still suffers from sluggish diffusion kinetics. A major obstacle that impedes Ca^{2+} insertion is its large ionic size, which results in a greater volume change and inducing severe structural distortion. The bivalency of Ca^{2+} also leads to stronger influence on the electronic structure to reach the local charge neutrality.[16,54] The hindrance implies a more complicated reaction pathway that makes reversible de-/calciation challenging. Moreover, Ca^{2+} suffers from considerably high desolvation energy barriers at the cathode-electrolyte interfaces, even higher than those of Mg^{2+}, leading to large overpotentials for Ca^{2+} intercalation.[55] To circumvent the desolvation process, solvent co-intercalation approaches were recently developed, which rendered improved Ca storage performance compared to conventional intercalation chemistries.[56] In fact, solvent co-intercalation can be seen as a competing process with bare Ca^{2+} intercalation at the electrode-electrolyte interfaces (Figure 7). While bare Ca^{2+} intercalation necessitates an energy-intensive desolvation step at the interfaces, co-intercalation bypasses the desovlation process, but needs to overcome the steric hindrance of large shuttling ions. Therefore, a strong solvating solvent is normally required to form a rigid solvation structure around Ca^{2+}. And to minimize the size effect, small solvent molecules are preferred. As for the host materials, large vacancies would be beneficial for accommodating the solvated cations. This is normally achieved by either applying hosts with flexible molecular layers, or adopting crystal engineer strategies to expand the lattice structure. The following section describes the development of both the anodes and the cathodes based on this principle.

4.1. Co-Intercalation Anode

When it comes to intercalation anodes, graphite is naturally a promising candidate, as it exhibits the capability of hosting various cation charge carriers and is applied as the anode materials for commercial LIBs.[57] Inspiringly, early study on Ca^{2+} intercalation into graphite revealed the process was thermodynamically favorable over Li^+. However, Ca-based binary graphite intercalation compounds (GICs) could only be obtained at high temperature of 350 °C by chemical

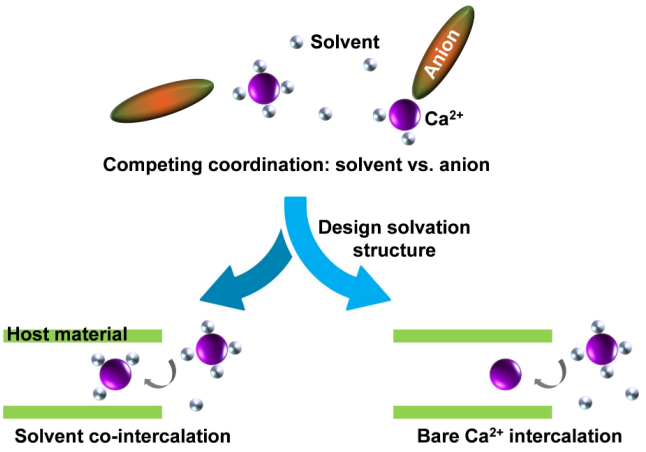

Figure 7. Schematic illustration of the competing processes between solvent co-intercalation and bare Ca^{2+} intercalation.

approaches, suggesting sluggish kinetics of the process.[58] Shifting from binary GICs to ternary GICs largely promoted the intercalation of Ca^{2+}. With the help of ethylenediamine (en), a ternary GICs $[Ca(en)_2]C_{26}$ could be prepared only at 40 °C.[59] This has motivated investigations on electrochemically co-intercalation of Ca^{2+} and solvent into graphite layers at ambient temperature.

In previous studies, solvent co-intercalation into graphite was already reported in Li, Na, K and Mg systems, demonstrating its feasibility to alkali and alkaline earth metal cations.[60] However, the reversibility of co-intercalation varies depending on the size of the charge carriers. While small cations (Li^+ and Mg^{2+}) showed limited reversibility for solvent co-intercalation, large cations (Na^+ and K^+) can efficiently stabilize the graphite structure, leading to excellent cycling stability and rate capability.[61] The feasibility of solvated Ca^{2+} intercalation into graphite was demonstrated in $Ca(TFSI)_2$-based electrolytes, with a capacitive activated carbon (AC) anode.[11b] While Ca^{2+} did not co-intercalate into graphite with alkylcarbonates nor short-chain glymes, it formed ternary GICs with tetraglyme (G4) to produce Ca–G4·C_{72}. The mechanism was studied by operando XRD, which indicated a multi-stage intercalation with a huge volume expansion up to 220 %, a typical feature of solvent co-intercalation.[57] Despite that, the graphite anode exhibited stable cycling for 2000 cycles and excellent rate capability up to 1 A g^{-1}, delivering a capacity of ~50 mAh g^{-1}. In a separate work, efforts were made to extend the concept to other electrolyte systems with solvents that are compatible with Ca metal anodes.[11a] Therefore, a $Ca(BH_4)_2$-based electrolyte was the subject of study, where dimethylacetamide (DMAc) enabled the intercalation of Ca^{2+} into graphite. As revealed by comprehensive spectroscopic and structural analysis, a stage II GIC $[Ca(DMAc)_4]C_{50}$ was formed, providing a reversible capacity of 87 mAh g^{-1} at 0.1 A g^{-1}.

Whether Ca^{2+} can co-intercalate into graphite host depends on the type of solvent applied. The success of G4 and DMAc with strong solvating power indicates that a rigid solvation structure of Ca^{2+} might be the key to realize co-intercalation. To regulate the solvation structure of Ca^{2+}, anions in the electrolytes is also playing a role. A recent study by Xu et al. revealed the association strength of anions as a descriptor for co-intercalation in graphite.[62] Anions that lead to an optimal coordination of four solvent molecules per Ca^{2+} render the highest reversibility and fastest kinetics. A coordination number (CN) of 4 is enough to shield the double charge of Ca^{2+}, but lower than the normal preferred CN of Ca^{2+} (6–8) in order to alleviate the size effect.[63]

4.2. Co-Intercalation Cathode

It should be noted that applying co-intercalation-based anode chemistry also induces large energy barrier for desolvation at the cathode interfaces (if without applying a co-intercalation cathode). A plausible approach to circumvent the issue is to establish a co-intercalation chemistry also for the cathode side,[64] where solvated Ca^{2+} are the charge carriers that shuttle between two electrodes. A proof-of-concept of co-intercalation batteries was recently demonstrated in sodium ion batteries (SIBs) using TiS_2 as cathode and graphite as anode.[65] In fact, Ca^{2+}-solvent co-intercalation into TiS_2 was reported, but the viability of the strategy was highly dependent on the type of electrolyte applied. It was found that the reversible electrochemical insertion of Ca in TiS_2 in $Ca(TFSI)_2$-PC electrolyte occurs through the formation of solvent co-intercalating phases at 100 °C, 60 °C, and room temperature.[66] The same phase was also observed at the initial calciation stage, by employing $Ca(BF_4)_2$/EC-PC electrolyte. However, deep calciation of TiS_2 leads to the formation of two non-co-intercalated phases.[67] The difference implies that the formulation of electrolyte is a critical factor, particularly the electrolyte structure and solvation energies etc. Furthermore, the abovementioned work also compared the electrochemical reduction of TiS_2 in the presence of Ca^{2+} and Mg^{2+}. When reduced in the presence of Mg^{2+} ($Mg(TFSI)_2$/EC-PC), only a Mg^{2+}-solvated intercalate was observed, whereby the fully dissociation and free Mg^{2+} cannot be intercalated. Interestingly, in a separate work, Sun et al. tested micrometer-sized TiS_2 electrode in APC/THF electrolyte versus Mg metal anode, which delivered a capacity of 115 mAh g^{-1} at a C/10 rate and 60 °C. Through in situ X-ray diffraction studies, the authors were able to identify multistep phase formation during Mg insertion into the TiS_2 structure, without solvent co-intercalation.[68] As ethereal solvents are the only type of solvent showing good compatibility with Ca metal anode, further investigation of co-intercalation in ether-based electrolytes would be promising.

Shifting to high-voltage cathode materials, solvent co-intercalation was already attempted in layered oxides in order to enhance Ca^{2+} diffusion, but mainly restricted to water as the co-intercalating agent. Sakurai et al. investigated Ca^{2+} intercalation in α-V_2O_5 from a $Ca(TFSI)_2$/EC-PC electrolyte, and found that the presence of water in the non-aqueous electrolyte improved the intercalation kinetics of Ca^{2+} by forming stable hydration shell around Ca^{2+}.[69] As water has a rather narrow electrochemical window, parasitic proton shuttling in the water-containing electrolyte was also evident. Nevertheless, X-ray diffraction (XRD) and inductive coupled plasma (ICP) analysis indicated only trace amount of proton co-intercalating with Ca^{2+}, which was different from the case of Mg^{2+}-water co-intercalation, where proton shuttling was dominant.[70] In fact, even reversible Ca storage in a copper hexacyanoferrate (CuHCF) cathode from an aqueous electrolyte was possible.[71] Although the degree of co-intercalation may vary depending on the test conditions (e.g. temperature),[72] the positive outcome mentioned above demonstrated the feasibility of water co-intercalation to enhance the storage of Ca^{2+}.

However, considering the compatibility with Ca metal anode, water-containing electrolyte is not a practical solution. An alternative approach that still applies the shielding effect of water is to introduce water as pillar in the layered compounds. These hydrated layered materials

provide larger interlayer spacing, which further facilitates ion diffusion. To this end, a hydrated $VOPO_4 \cdot 2H_2O$ structure with interlayer distance of ~7.41 Å was reported, which was expanded by 70 % from its anhydrate phase.[73] The cathode delivered a reversible capacity of ~100 mAh g^{-1} with an average voltage of 2.8 V vs Ca for 200 cycles. Interestingly, a structural shrinkage by ~14 % along c-axis upon Ca^{2+} intercalation was observed in operando XRD patterns, which indicated a strong interaction between Ca^{2+} and the pillaring water. A similar contraction of the interlayer spacing was also evident in a calcium molybdenum bronze $Ca_xMoO_3 \cdot yH_2O$ cathode[74] and in a metahewettite vanadium oxide $CaV_6O_{16} \cdot 2.8H_2O$ cathode[75] after calciation. To further enhance the structural stability, a bilayer $Mg_{0.25}V_2O_5 \cdot H_2O$ compounds was developed (Figure 8a). By employing Mg^{2+} as co-pillar, the cathode allowed 0.36 Ca^{2+} uptake per formula unit with only 0.8 % interlayer expansion, leading to a stable cycling up to 500 cycles (with capacity retention of 86.9 %).[76]

Nevertheless, the strong interaction of Ca^{2+} with crystal water still raised concern on possible water shuttling together with Ca^{2+}, which is detrimental to the metal anode. To completely replace water, dry organic electrolyte with strong chelating agent as additive was applied. It was found that methoxyethylamine chelants with heterogeneous donor atoms provided a flexible solvation structure to Ca^{2+}.[77] Despite of a larger size, these chelated Ca-ions were able to adjust their solvation configuration during intercalation as illustrated in Figure 8b. Therefore, solvated Ca^{2+} intercalation into a layered $Mg_{0.15}MnO_2$ cathode exhibited high reversibility and allowed coupling with a metallic Ca anode. The respective cell showed an average output voltage of 2.6 V, delivering a capacity of 210 mAh g^{-1} at 0.5 C for 50 cycles with almost no capacity fading (Figure 8c).[77] The preliminary evaluation demonstrated a highly promising Ca battery cell with an energy density that is comparable to the state-of-the-art $LiFePO_4$ cathode in LIBs, which deserves further systematic investigation.

Beyond solvent co-intercalation, other co-intercalation strategies such as anion co-intercalation and cation co-intercalation strategies are also promising.[78] As developed in Mg systems, strong chelating anions (such as Cl^-) form complexes with Mg^{2+} in the electrolyte, and can intercalate as a whole into the host materials (anion co-intercalation).[79] In such a way, the charge density of the carriers is significantly reduced, giving rise to faster diffusion kinetics. However, introducing Cl^- into Ca electrolyte is not straightforward, as it easily precipitates in the form of $CaCl_2$.[5] Whereas, cation co-intercalation improves the diffusion kinetics with the help of an assisting monovalent cation, which is more mobile than the multivalent charge carriers. A proof-of-concept study by our group demonstrated that the cation co-intercalation could enhance Mg storage in conventional layered compound by >50 %.[80] In fact, a concerted motion between Ca^{2+} and Na^+ in $NaV_2(PO_4)_3$ was recently reported by Nazar et al.[81] However, whether co-intercalation of monovalent cation improves Ca storage requires further validation.

5. Size Effect & Site Preference

Pioneering work to explore viable cathode chemistry for Ca-based batteries was carried out on layered compounds, which are natural hosts for various charge carriers due to the weak interlayer force between their molecular slabs.[82]

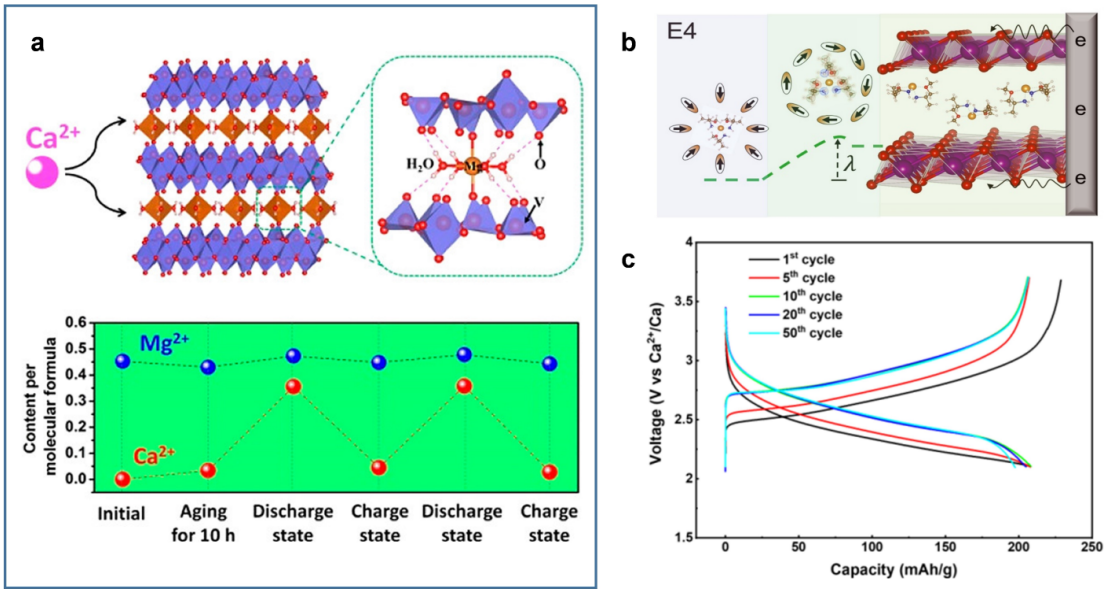

Figure 8. (a) Ca^{2+} intercalation into a bilayer $Mg_{0.25}V_2O_5 \cdot H_2O$ cathode and the respective Ca content at different states of charge. Reproduced with permission.[76] Copyright 2019, American Chemical Society. (b) Schematic illustration of the solvation sheath reorganization that promotes interfacial transport. (c) Cycling performance of $Mg_{0.15}MnO_2$/Ca[B(hfip)$_4$]$_2$-diglyme/Ca cell with methoxyethyl amine as electrolyte additive. Reproduced with permission.[77] Copyright 2021 the Authors. Published by American Association for the Advancement of Science.

Early studies demonstrated the feasibility to reversibly de-/intercalate Ca^{2+} into typical 2D transition metal chalcogenides such as V_2O_5 and MoO_3 etc.[82a,b,83] This is in sharp contrast to Mg storage in these materials, which normally triggered significant Mg^{2+} trapping and severe structural degradation.[67–68,84] The enhancement in the solid diffusion kinetics was attributed to the reduced charge density of Ca^{2+} compared to Mg^{2+} as previously mentioned. Nevertheless, structural investigations revealed more frequent and complicated phase transitions of the layered materials upon taking up Ca^{2+}.[67,82b,83b] A possible reason for this characteristics is the size effect, where large Ca^{2+} prefers prismatic coordination over octahedral coordination to minimize the repulsion between the guest cations (Figure 9a).[17] Based on these findings, transition metal oxides with promising crystal structures were theoretically predicted and some of them being experimentally evaluated.

On the other hand, the size effect and the preferential prismatic coordination are similar features for Ca^{2+} (r = 1.14 Å) and Na^+ (r = 1.16 Å), and might be generalized to other host structures beyond the layered materials. To this end, viable cathodes that are already developed in SIBs could be potential candidates for the storage of Ca^{2+}. In particular, open framework (OF) structures such as Prussian blue analogs, NASICONs etc. provide large diffusion channels in three-dimensions, which are capable of hosting various intercalants including multivalent cations.[85] Typical OF structures are made from either "inorganic" clusters or isolated metal ions that are bridged by multitopic ligands through (quasi−)covalent bonding, which ensures rigid crystal structure against reversible de-/insertion of the guest cations.[86] These materials exhibited excellent Na storage performance in terms of cycling stability as well as rate capability, and have been developed as cathode materials for commercial SIBs.[87] The success in SIBs motivated research activities to investigate Ca storage in the OF structures.

As the state-of-the-art, some desired compounds of the above-mentioned material classes already demonstrated reversible Ca^{2+} de-/insertion. And these materials could practically provide an energy density around 300 Wh kg^{-1} at material level (Figure 9b). Therefore, this section mainly focuses on the size effect and site preference of Ca^{2+}, and its similarity with Na^+. Transition metal oxides, and OF structures such as Prussian blue analogues and polyanion compounds will be main topics of discussion.

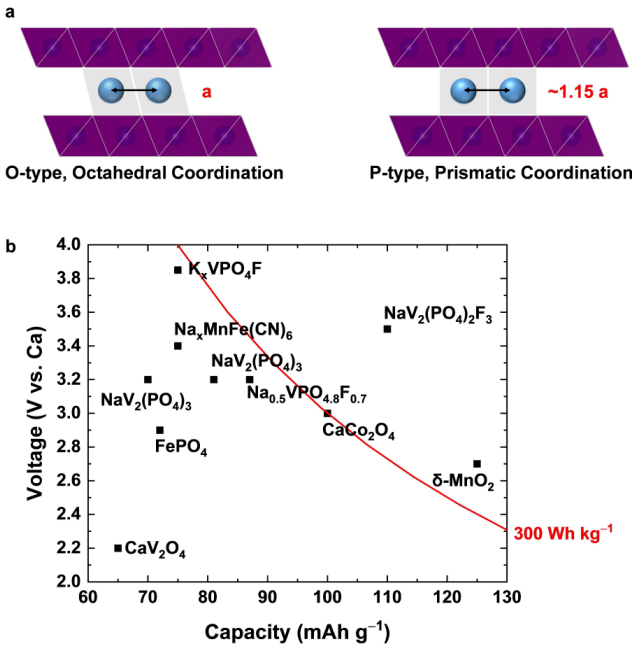

Figure 9. (a) Comparison of distance between neighbouring guest cations in O-type and P-type layered transition metal chalcogenides. (b) Representative cathode materials investigated for Ca-based batteries.[13,44,88]

5.1. Transition Metal Oxides

Till now, only few transition metal oxides and cathode hosts in general have been experimentally investigated, from which the understanding of Ca chemistries such as the thermodynamic preference and transport properties of Ca^{2+} are still lacking. However, theoretical studies and computational screening on the oxide cathodes were progressively reported with a number of promising structures being proposed. By applying first-principle calculations, Zapol et al. systematically evaluated layered $CaTM_2O_4$ compounds with first-row transition metals in different stacking sequences.[89] It was found that Ca^{2+} with a large ionic radius prefers prismatic coordination, thereby P-type $CaTM_2O_4$ structures exhibited both thermodynamic and kinetic advantages for Ca storage. The predicted energy barrier for Ca^{2+} diffusion within the $P1$ and $P2_1/m$ polymorphs at high vacancy limit were only around 300 meV.[89] However, its migration in O3 stackings requires to overcome a 750 meV energy barrier, which is more than doubled.[90] In addition, intercalation of Ca^{2+} in P-type layered compounds was thermodynamically favorable over the conversion reactions for most of the studied compounds. Among different TM substitutes, $CaCo_2O_4$ exhibited the best balance of electrochemical properties including thermodynamic stability, average voltage, energy density, ionic mobility etc.[89] The theoretical findings were in fairly good agreement with experimental results, where $CaCo_2O_4$ cathode was tested against a V_2O_5 counter electrode in a $Ca(ClO_4)_2$/ACN electrolyte. At 50 μA, the $CaCo_2O_4$ cathode delivered a capacity close to 100 mAh g^{-1}.[88b]

In addition to $CaCo_2O_4$, other oxide structures were also investigated, among which Ca-Mn–O system was the most intensively studied due to the high abundance of Mn as well as the structural versatility of MnO_2. Common MnO_2 polymorphs include hollandite (α), pyrolusite (β), intergrowth (γ), birnessite (δ), and spinel (λ) structures, depending on how the MnO_6 octahedral building blocks are connected.[91] These MnO_2 compounds are normally produced via solution chemistry approaches, leading to the containing of water molecules or other small cations as structural pillars within the lattice.[92] In addition, water-free

layered MnO_2 polymorphs such as P3-type or O2-type Ca_xMnO_2 may also exist, similar to the corresponding Na analogues.[93] Due to the sluggish ion mobility, reversible Ca^{2+} intercalation into the water-free Ca_xMnO_2 has not yet been reported. However, a systematic DFT study of the water-containing MnO_2 polymorphs for Ca storage was carried out by Juran et al., who found both α-MnO_2 (hollandite phase, 0.19 eV) and δ-MnO_2 (layered, 0.55 eV) showed fairly low diffusion energy barrier during Ca^{2+} intercalation.[94] This was further confirmed by experiments, where both MnO_2 polymorphs enabled reversible Ca^{2+} storage, however, δ-MnO_2 exhibited higher capacity and better rate capability.[88c] Nevertheless, gradual capacity fading was evident after only 20–30 cycles, which was attributed to manganese dissolution. The result is in sharp contrast to Na^+ storage in δ-MnO_2, where the interlayer pillars could well stabilize the structure by suppressing the Jahn–Teller distortions.[95] The comparison might hint at more severe structural distortion upon Ca^{2+} intercalation. Moreover, the structure water could be extracted during cycling, which deteriorates the storage performance.[93] Besides the layered structures, Mn-based spinel oxides also showed promising storage properties. Based on the calculation from Liu et al., Ca storage in Mn_2O_4 spinel exhibited a low diffusion barrier close to that for Li^+ and at the same time providing a high energy density.[96] However, it should be noted that the predicted fast mobility is benefited from the fact that Ca^{2+} occupies an unfavorable tetrahedral site, which leads to the formation of a metastable phase. Whether and how the Ca-containing Mn_2O_4 spinel compounds can be synthesized needs further experimental validation. On the other hand, the thermodynamically stable phase marokite $CaMn_2O_4$ (also known as post spinel phase) presents promisingly high voltage and small volume change upon Ca extraction.[97] However, the diffusion of Ca^{2+} has to overcome a kinetic barrier as high as 1 eV, making it challenging to access the redox at moderate test conditions. Substituting Mn with V leads to a substantial decrease of the diffusion barrier to 0.65 eV.[98] As a result, the CaV_2O_4 post spinel structure exhibited promising cycling in a $Ca(BF_4)_2$/EC-PC electrolyte, by hosting 0.25 mole Ca^{2+} per formula unit at room temperature and up to 0.6 Ca^{2+} at 50 °C.[88d]

Despite the progress, there is still lack of viable oxide compounds that accommodate Ca^{2+} at fair charging rate, which highlights the sluggish diffusion kinetics as a remaining issue. Nevertheless, computational analysis proved to be an efficient tool for early-stage screening from a large material database. As high-performance Ca electrolyte is still lacking, modelling of Ca^{2+} diffusion in the host structures avoids unwanted side reactions with the electrolyte, which are likely to encounter in experiments and may mask the real performance of tested materials. Therefore, combinatory approaches involving experimental, theoretical predictions, and artificial intelligence may eventually lead to significant breakthroughs in the field of Ca cathodes.

5.2. Prussian Blue Analogues (PBAs)

The first OF structures reported to reversibly insert Ca^{2+} are the Prussian blue family with a general formula $A_xMM'(CN)_6 \cdot yH_2O$, where A is the guest cation, and M and M' stands for transition metal located at corners and edges of the cubic lattice, respectively. Among them, nickel hexacyanoferrate (NiHCF) was of particular interest as it showed zero-strain feature (negligible volume change) upon Na^+ insertion, which was beneficial for reversibly hosting large cations.[99] To this end, a NiHCF cathode was studied in a calcium nitrate water solution, demonstrating unprecedented cycling stability of >2000 cycles. Note, the excellent reversibility was likely partially associated with the hydration shell around the intercalants, which boost the solid diffusion kinetics of Ca^{2+} by screening their double charge. In any case, the NiHCF cathode provided a redox potential of ~0.7 V vs. SHE in the aqueous Ca electrolyte, corresponding to ~3.6 V vs. Ca.[100]

However, such promising redox potential can hardly be transferred into a high cell voltage in aqueous Ca batteries, due to the narrow electrochemical window of H_2O, and the incompatibility between aqueous electrolyte and Ca metal anode.[101] To unlock the limit, Ca insertion into the NiHCF from a non-aqueous electrolyte $Ca(PF_6)_2$ in EC/PC was tested.[102] The cathode delivered an initial capacity of 60 mAh g^{-1}, which degraded to ~50 % after 20 cycles. Multimodal analysis confirmed the reversible Ca^{2+} shuttling, which triggered Fe^{2+}/Fe^{3+} redox but leaving Ni electrochemically inactive. Substituting Ni by another redox active transition metal Mn led to a slightly increase of the capacity to 75 mAh g^{-1}, which is only ~50 % of the value in SIBs (Figure 10a–b).[44] Interestingly, XANES investigation indicated Mn to be the solely redox center in the MnHCF, while the oxidation state of Fe is unchanged during Ca^{2+} insertion (Figure 10c–d). In comparison, both Fe and Mn were

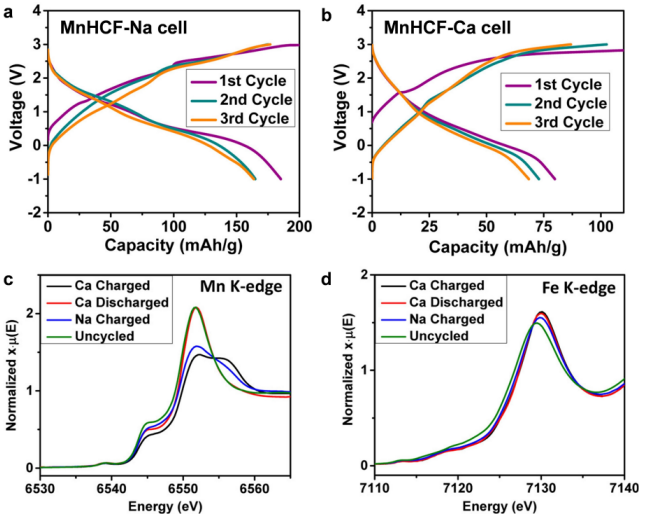

Figure 10. (a) Na^+ and (b) Ca^{2+} insertion into the MnHCF cathode. (c, d) XANES Mn K-edge and Fe K-edge of the MnHCF cathode at different states of charge. Reproduced with permission.[44] Copyright 2015, American Chemistry Society.

changing their oxidation states upon Na storage in the same cathode, amounting to a doubled capacity. In another study, Fe was introduced to replace Ni in the Prussian blue structure.[103] The resultant FeHCF provided an increased capacity of 100 mAh g^{-1}, which seemed to activate Fe redox at both sites. However, a detailed structural analysis is still pending to clarify the storage mechanism. In order to increase the energy density of the PBA cathode, further efforts could be considered to develop approaches that trigger all the redox active transition metals in the PBAs, so that a high capacity/energy can be achieved.

5.3. Polyanion Frameworks

Polyanion compounds represent another typical OF structure, consisting of polyanion tetrahedra (such as $[PO_4]^{3-}$ and $[SiO_4]^{4-}$) or their derivatives $[X_mO_{3m+1}]^{n-}$ (X = S, P, Si, As, Mo, or W) and transition metal oxide polyhedral MO_x.[104] These materials provide a stable covalent network with fast-kinetic diffusion channels for guest cations. Compared to –CN ligand in the PBAs, polyanion tetrahedron possesses a higher thermal stability and lower toxicity.[105] In addition, there are strong X–O bonds in the polyanion units, which give rise to a so-called inductive effect on the MO_x polyhedra that lifts up the redox potential of transition metal to a value similar to or even higher than that in the PBAs.[106]

Among the polyanion family, NASICON-type compounds offer one of the highest Na^+ diffusivities. They were used as cathode materials but also as solid electrolyte for Na-based batteries.[107] Considering the similar ionic radius between Na^+ and Ca^{2+}, NASICON-type $NaV_2(PO_4)_3$ (NVP) was recently investigated as a cathode host for RCBs.[13a,88e] Chemical calciation of NVP led to 0.8 Ca^{2+} uptake, demonstrating its thermodynamic feasibility to host Ca^{2+}.[88e] This process could also be driven electrochemically by cycling NVP in a $Ca(TFSI)_2$/diglyme electrolyte, leading to reversible de-/calciation of 0.5 Ca^{2+} per formula unit. In spite of a phase change at high cation content, the NVP cathode could be cycled reversibly for 40 cycles, providing a capacity of 83 mAh g^{-1} at 3.25 V vs. Ca (Figure 11a). However, fine structure characterizations demonstrated a limited penetration depth of Ca^{2+} into the bulk (tens of nm, Figure 11b), suggesting kinetic hindrance as a remaining issue even at a low current density of 3.5 mA g^{-1}.[13a] Furthermore, insertion of Ca^{2+} into NVP seemed sensitive to the electrolyte. While Ca^{2+} was clarified as the major charge carrier in case of the glyme-based electrolyte,[13a] Na storage was dominant with negligible Ca^{2+} contribution when using a carbonate-based electrolyte.[88e] The dependence of Ca storage on different electrolytes remains elusive as glymes have stronger coordination strength than carbo-

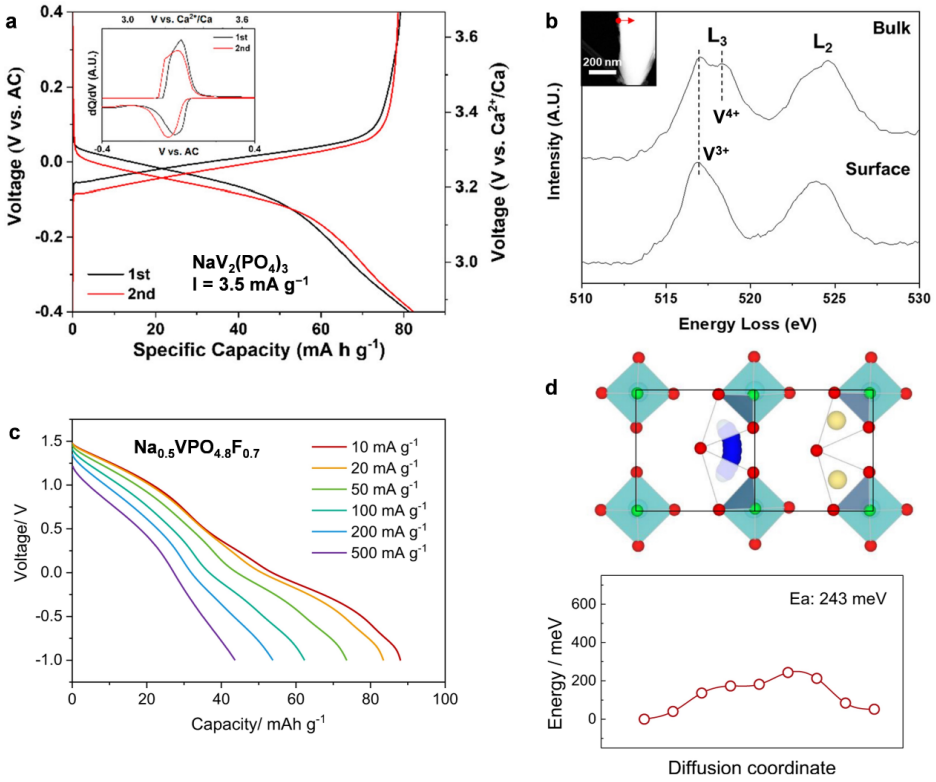

Figure 11. Ca^{2+} de-/insertion in $NaV_2(PO_4)_3$: (a) voltage profiles; (b) EELS probing oxidation state change of V at the surface and in the bulk of the active particle. Reproduced with permission.[13a] Copyright 2020, American Chemistry Society. Ca^{2+} de-/insertion in $Na_{0.5}VPO_{4.8}F_{0.7}$: (c) discharge profiles at various current rate; (d) intra-unit hopping of Ca^{2+} and the corresponding energy profile. Reproduced with permission.[13b] Copyright 2021, the Authors, published by Springer Nature.

nates and therefore a higher desolvation energy barrier would be expected. This calls for more efforts to understanding the transport mechanisms at cathode-electrolyte interfaces.

On the basis of the NVP structure, further crystal engineering approaches were applied to optimize the chemical environment of the diffusion channels. By partially substituting PO_4 with O and F, the $Na_{1.5}VPO_{4.8}F_{0.7}$ (NVPF) exhibited one of the lowest volume change (~2.9 %) during de-/sodiation, which alleviated the capacity fading caused by structural degradation to the minimum.[108] More importantly, the host structure rendered fast Na^+ diffusion with activation barriers of only 30–300 meV, which is similar to those of layered oxides for LIBs (e.g. $LiCoO_2$).[108] To investigate the Ca storage performance, $Na_{1.5}VPO_{4.8}F_{0.7}$ was first desodiated electrochemically. In a separate cell, the resultant $Na_{0.5}VPO_{4.8}F_{0.7}$ cathode was tested in a $Ca(PF_6)_2$/EC-PC electrolyte, exhibiting excellent reversibility (90 % capacity retention after 500 cycles) and rate capability (up to 500 mA g^{-1}, Figure 11c) upon uptaking and releasing Ca^{2+}.[13b] High resolution XRD with Rietveld refinement indicated a similar site preference for Na^+ and Ca^{2+}, and Ca^{2+} insertion led to even smaller volume expansion of 1.4 %, which well-explained the superior cycling stability. Whereas the excellent rate capability could be attributed to the low diffusion barrier of only 243 meV for Ca^{2+} hopping through an intra-unit pathway (Figure 11d). The success in NVPF motivated further research activities to optimize the host structure. In fact, the $Na_{1.5}VPO_{4.8}F_{0.7}$ belongs to the family of $Na_3(VO_{1-x}PO_4)_2F_{1+2x}$, which well-maintains their crystal phase in the range of $0 \leq x \leq 1$.[109] Due to a similar inductive effect of F, the average redox potential of $V^{3+}/V^{4+}/V^{5+}$ could be increased to 3.5 V vs. Ca in a fully fluorinated compounds $NaV_2(PO_4)_2F_3$ ($x=1$).[88a] In a model cell setup using AC anode, the $NaV_2(PO_4)_2F_3$ cathode provided a stable Ca storage capacity of 80–90 mAh g^{-1} for 2000 cycles. With a similar structure, a K_xVPO_4F (x~0) cathode delivered a capacity of ~75 mAh g^{-1} at a high voltage of 3.85 V vs. Ca, and even enabled stable cycling against a Ca metal anode (70 % retention after 40 cycles). Again, the excellent cycling performance was correlated with a small volume change upon Ca^{2+} de-/insertion ($\Delta V = 1.9$ %). To further exploit the structural features, other NASICON compounds or fluorophosphates framework in general would be promising and deserve further development as cathode materials for RCBs.

Beyond NASICON compounds, other polyanion cathodes that offer large diffusion channels were also evaluated. Intercalation of Ca^{2+} into a layered Na_2FePO_4F was reported to take place at 2.6 V in a carbonate-based electrolyte, delivering a capacity of 80 mAh g^{-1}.[110] In order to increase the capacity, efforts were made to reduce the content of polyanion in the structure that is electrochemically inactive.[13a,32] The resultant $FePO_4$ cathode was able to deliver a capacity of 120 mAh g^{-1}, which is ~50 % higher than other OF structures reported so far. By applying the state-of-the-art $Ca[B(hfip)_4]_2$/diglyme electrolyte, the $FePO_4$ cathode was able to cycle against a Ca metal anode for 10 times, resulting in a cell voltage of 3.4 V.[32] Despite severe overcharging probably due to electrolyte degradation, the preliminary evaluation afforded research opportunities for achieving practical high-energy Ca batteries.

6. Organic Redox Chemistries

Organic compounds are mainly composed of abundant elements such as C, O, H, N, S etc. providing a sustainable solution to shift away from the dependence on transition metals. Compared to rigid inorganic crystal frameworks, organic compounds with redox-active functional groups are typically less ordered, rendering flexible molecular structures for fast ion mobility and easy access to the redox centers.[111] Furthermore, storage mechanisms of these materials are based on coordination chemistry, which has weaker interaction between the redox center and the charge carrier. Benefiting from the thermodynamic and kinetic advantages, redox-active organic cathodes feature high reversibility and excellent rate capability.[112] Therefore, redox-active compounds developed in other batteries were also tested in Ca batteries. They are mostly with either carbonyl groups or amine groups, which represent n-type (coordination to Ca^{2+}) or p-type (interaction with anions) cathodes, respectively. Typical n-type and p-type compounds investigated in Ca-based batteries are presented in Figure 12a.

6.1. N-Type Compounds

As a starting point, efforts were made focusing on conjugated carbonyl compounds like polyanthraquinone-based cathodes, whose charge storage mechanisms were well-understood in Mg batteries.[113] In Mg batteries, 1,4-polyanthraquinone (14PAQ) exhibited the best cell performance among various polyanthraquinone isomers and polyanthraquinonyl sulfide (PAQS).[114] It was therefore tested in Ca metal batteries applying the $Ca[B(hfip)_4]_2$/DME electrolyte. Ex situ IR spectra indicated a reversible enolization reaction of the carbonyl groups in the 14PAQ (Figure 12b), similar to the case of Mg^{2+} storage,[115] which provided a plateau at 2.0 V and an initial capacity of ~250 mAh g^{-1}.[12b] However, a substantial increase of the overpotential for initial Ca stripping process at each cycle led to a sudden drop of the cell capacity only after a few cycles, reflecting severe passivation of the metal anode. To avoid anode passivation, electrochemical test of the 14PAQ was performed against a Ca–Sn alloy anode, which exhibited significantly improved cycling stability compared to Ca metal anode.[116] Benefiting from that, the real performance of the 14PAQ cathode was revealed, showing similar initial capacities (Figure 12d) and an extraordinarily long lifespan of 5000 cycles with a capacity retention of 78 mAh g^{-1}.

Compared to 14PAQ, PAQS can be synthesized in a more cost-effective manner, which makes it more promising for upscaling. Bitenc et al. carried out electrochemical and mechanistic study of Ca metal organic battery by coupling a PAQS cathode with the $Ca[B(hfip)_4]_2$/DME electrolyte.[117] Initial test of the plain PAQS polymer showed large voltage

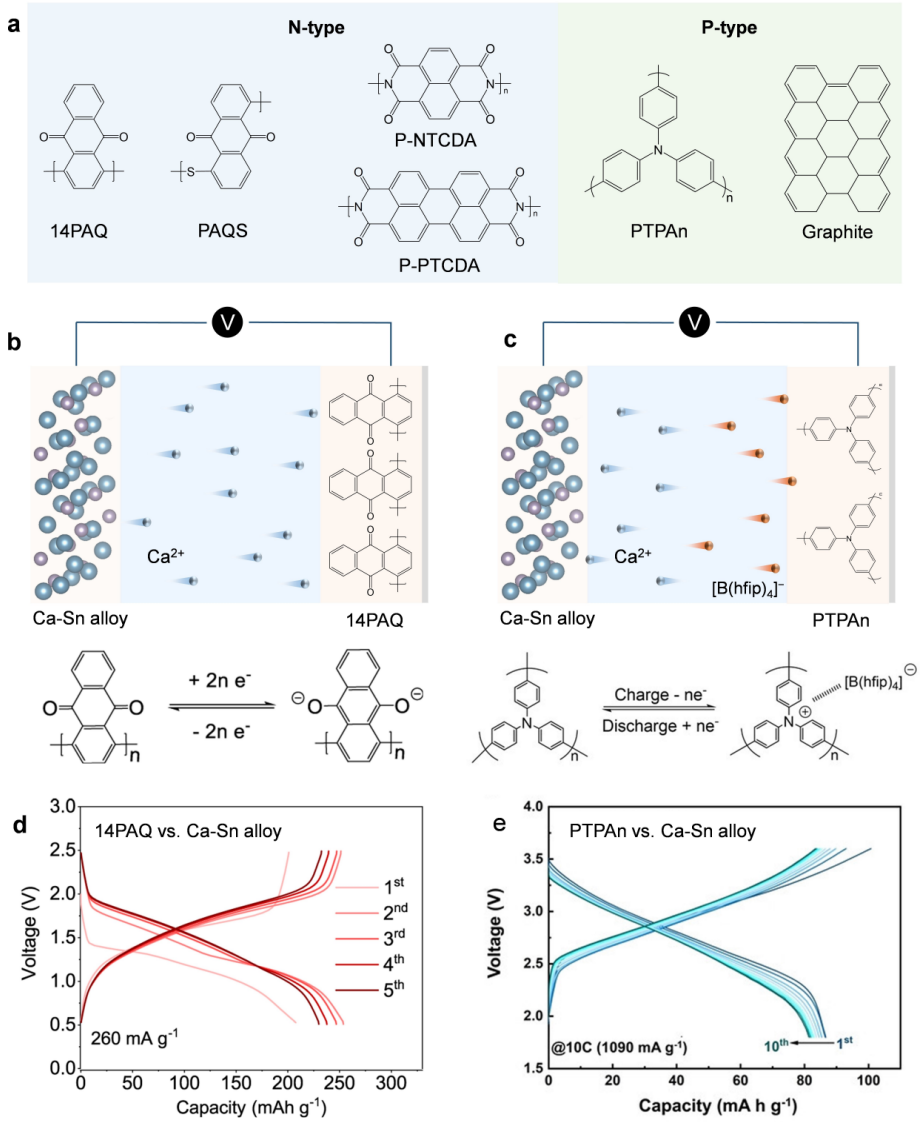

Figure 12. Polymer cathodes for Ca-based batteries: (a) typical n-type and p-type polymers; (b) n-type and (c) p-type cell configurations and the respective cathode reactions; voltage profiles of the (d) 14PAQ and (e) PTPAn cathodes vs. Ca Sn alloy anode. (b) and (d) Reproduced with permission.[12b] Copyright 2022, the Authors, published by Springer Nature. (c) and (e) Reproduced with permission.[46] Copyright 2023, the Authors, published by Wiley.

hysteresis and low redox activity providing only 20 % its theoretical capacity, hinting at low electronic conductivity of the material. To enhance the charge transfer, PAQS was in situ polymerized in a CNT matrix. The resultant PAQS/CNT composite exhibited an improved capacity of 170 mAh g^{-1} (75 % utilization of the active material). Reversible redox of the carbonyl groups and their interaction with Ca^{2+} were confirmed by IR spectra and EDX analysis. However, undesired storage of the monovalent ion pairs ($Ca[B(hfip)_4]^+$) was also revealed. The cation-anion co-insertion in polymer cathodes was also found in Mg batteries,[118] which may be avoided by a proper design of the solvation structure in the electrolyte. In addition, early cell failure due to the passivation of Ca metal anode was also the case with the PAQS/CNT cathode. To have a fair evaluation of the PAQS-based cathode, it was measured in model systems comprised of activated carbon (AC) as counter electrode, with Ag^+/Ag couple as internal reference.[119] In a carbonated-based $Ca(TFSI)_2$ electrolyte, the PAQS/CNT composite cathode exhibits high rate performance and stable cycling up to 500 cycles (83 % capacity retention). Motivated by that, PAQS/C composite cathodes were further cycled against Ca–Sn alloy anodes.[120] In this cell configuration, the PAQS/C cathode delivered maximum capacity of 83 mAh g^{-1} at 0.5 C, with a capacity retention of 45 mAh g^{-1} after 1000 cycles.

Due to the low electronic conductivity of the polyanthraquinone-based compounds, other carbonyl structures with enhanced conjugation were investigated. In this regard, a comparative study was carried out on three dianhydrides monomers, namely pyromellitic dianhydride (PMDA), 1,4,5,8-naphthalenetetracarboxylic dianhydride (NTCDA),

and 3,4,9,10-perylenetetracarboxylic dianhydride (PTCDA), with increasing number of aromatic rings.[121] The plain monomer cathodes delivered initial capacities all above 100 mAh g^{-1} with discharge plateau at ~2.5 V. However, fast capacity fading was evident, indicating strong dissolution of the reduced species. To enhance the cycling stability, the monomers were transformed into the respective polyimides by reacting with amines. Electrochemical investigation on the polyimides revealed 34 % and 55 % utilization of the active material in P-NTCDA and P-PTCDA, respectively. Both values are higher than the case of PAQS (20 %), demonstrating the feasibility of the strategy. However, as the aromatic rings do not contribute to the capacity, rational design of the carbonyl compounds requires a balance between their π-structure and the redox-active content. Another approach to alleviate the dissolution is applying concentrated electrolyte. By using a saturated $Ca(ClO_4)_2$/PC electrolyte, the PTCDA could be cycled for 500 times with 80 % capacity retention.[122] On the other hand, a recent study compares electrochemical performance of the P-NTCDA cathode in Li/Na/Mg/Ca cells.[123] While the polyimide cathode provided a capacity of 90 and 45 mAh g^{-1} in Ca and Mg systems, respectively, higher capacities >135 mAh g^{-1} were achieved in monovalent batteries. One possible reason for the low utilization of active material in divalent systems is the prominent solvation and ion-pairing effect in the respective electrolyte, which leads to storage of large ion clusters (e.g. $Ca[B(hfip)_4]^+$) instead of Ca^{2+}. To tackle this issue, electrolyte engineering could be effective.

6.2. P-Type Compounds

In addition to the n-type carbonyl compounds, p-type materials were also investigated. P-type cathodes mainly include tertiary amines that attract Ca^{2+} by Coulombic interaction, or graphite materials which intercalate anions in the electrolyte (Figure 12c). Both the redox of tertiary amine groups and the anion intercalation typically take place at high voltages >3 V vs. Ca. Such p-type compounds are normally used in dual-ion cell configuration where anions of electrolyte are shuttling at cathode side while Ca^{2+} stored at anode side. Based on the performance of p-type polymers in Mg batteries, polytriphenylamine (PTPAn) cathode was investigated. As revealed by Zhang et al., the storage performance of PTPAn varied with different Ca electrolytes. Among others, $Ca(TFSI)_2$/G4 electrolyte exhibited the best cycling performance, probably due to its fast diffusion coefficient and low binding energy with N center. On the other hand, the choice of anode also plays a role. In Ca metal batteries, the PTPAn cathode provided initial capacities of 80 mAh g^{-1} at 3.5 V. However, the capacity decreased sharply after 20 cycles, due to the passivation of the metal anode. Replacing the Ca anode by $CaSn_3$ alloy anode improved the cycling stability significantly. Despite a lowered average voltage of ~2.8 V (Figure 12e), the cell could be cycled for 3000 times with 60 % capacity retention. Inspired by that, PTPAn was further tested against polyimide anodes. This resulted in a Ca-based all-organic dual-ion batteries, which might feature low-cost and sustainability. Remarkably, the cell exhibited superior low temperature performance, due to the fast kinetics of both the cathode and anode reactions.[124] In a similar manner, a graphite anode was employed. The graphite anode was able to intercalate solvated Ca^{2+} to form a ternary graphite co-intercalation compound with fast kinetics. Compared to the polyimide anode, the storage of Ca^{2+} in graphite occurs at a lower potential, thereby a high cell voltage can be achieved. As a result, the PTPAn-graphite cell showed excellent cycling of 2000 times, with an operation voltage of 2.7 V. As mentioned, the graphite could also intercalate anion in the electrolyte. To exploit the high redox potential of anion intercalation, metallic Sn anode based on Ca–Sn alloying processes was applied.[125] The graphite-Sn cell demonstrated excellent cycling stability and rate capability, it also delivered a promising average cell voltage >4 V.

Overall, organic compounds so far exhibit the best storage performance in Ca batteries. There are lots of similarities between the storage of Ca^{2+} and Mg^{2+}, e.g. due to their divalency which makes it more difficult for local charge compensation. The divalent ions also have strong solvation energy and large solvation structures, which lowers the accessibility to the redox centers. This means other organic cathodes developed in Mg batteries could be also promising for Ca batteries. On the other hand, the above-mentioned issue calls for mutual development with the electrolyte. In addition, there are more organic compounds already reported in aqueous Ca electrolyte.[126] Their performance in non-aqueous electrolytes deserves further evaluation.

7. Conversion Compounds

Like in Mg batteries,[78] another pathway to bypass the slow solid-state diffusion of Ca-ions is the utilization of conversion cathodes.

Cathode materials that follow a conversion mechanism normally enable multi-electron redox reaction delivering high capacity/energy, but additionally feature sustainability and cost-efficiency by using earth-abundant elements and non-critical materials. Compared to intercalation compounds, reports on conversion materials for Ca batteries are rather scarce and only comprise elemental chalcogens (oxygen, sulfur and selenium), elemental halogens (chlorine), as well as the corresponding chalcogenides like CuS and FeS_2.

7.1. Elemental Sulfur

Elemental sulfur (S) is a typical conversion cathode material, which provides a two-electron reaction as described in Table 1. The formation of calcium sulfide (CaS) from elemental S and metallic Ca has a gibbs energy ($\Delta_r G$) of -477.4 kJ mol^{-1}, resulting in a theoretical cell voltage of 2.47 V, which is even higher than that of Li–S batteries (2.20 V). The Ca–S battery could theoretically provide a volumetric energy density of 3151 Wh L^{-1} (1806 Wh kg^{-1} on

Table 1: Comparison of different metal-sulfur chemistries.

Electrochemical reaction	$\Delta_r G$ kJ mol^{-1}	EMF V	Capacity mAh g^{-1}	Capacity mAh cm^{-3}	Energy density Wh kg^{-1}	Energy density Wh L^{-1}
$2Li + S \leftrightarrows Li_2S$	439.0	2.20	1672 (S)	3460 (S)	2570 (2Li + S)	2830 (2Li + S)
$Mg + S \leftrightarrows MgS$	341.8	1.77	1672 (S)	3460 (S)	1694 (Mg + S)	3227 (Mg + S)
$Ca + S \leftrightarrows CaS$	477.4	2.47	1672 (S)	3460 (S)	1806 (Ca + S)	3151 (Ca + S)

a weight basis), which is comparable to that of a Mg–S system, yet beyond that of a Li–S battery (2830 Wh L^{-1}).[127] Analogous to Mg–S cells, the likely passivation of the metal anode and the sluggish redox kinetics of the sulfur conversion represent the main hurdles towards its realization. In an early work by See et al. in 2013, a proof-of-concept Ca–S battery was reported applying $Ca(ClO_4)_2$ in different solvents like acetonitrile and DME.[128] However, due to the limited anodic stability of the perchlorate electrolyte and consequent passivation of the Ca anode, only primary Ca–S cells could be achieved.

Both studies face a rapid capacity decay with approx. 200 mAh g^{-1} after 15 cycles and subsequent cell failure – probably due to Ca anode passivation. Compared to Mg–S cells, the voltage hysteresis is surprisingly small (Figure 13a–c), which points to the sulfur redox kinetics being faster with the larger Ca^{2+} ion than the charge-denser Mg^{2+} ion.

To further enhance the kinetics, hybrid electrolytes comprising an additional monovalent salt can be utilized. With no other monovalent ion reservoir than the electrolyte, such approach requires high reversibility. This concept refers to Daniell-type cells in which the cathode reaction of the monovalent cation (e.g. Li^+) is kinetically favored, while Ca plating/stripping at the anode is thermodynamically preferred.[78] Thus, only elements with lower redox potential than Ca metal (−2.87 V), namely Li (−3.04 V) and K (−2.93 V), can be applied. In contrast, Mg metal (−2.37 V) also allows the use of a hybrid electrolyte comprising Na ions (−2.71 V). Actually, the discharge cell voltage in Ca–S (approx. 2.1 V) and Mg–S cells (approx. 1.5 V) is already close to its thermodynamic value (2.47 V and 1.77 V, respectively) – and in fact lowered by Li salt addition (Figure 13d–e), which is at least unexpected in case of Mg–S

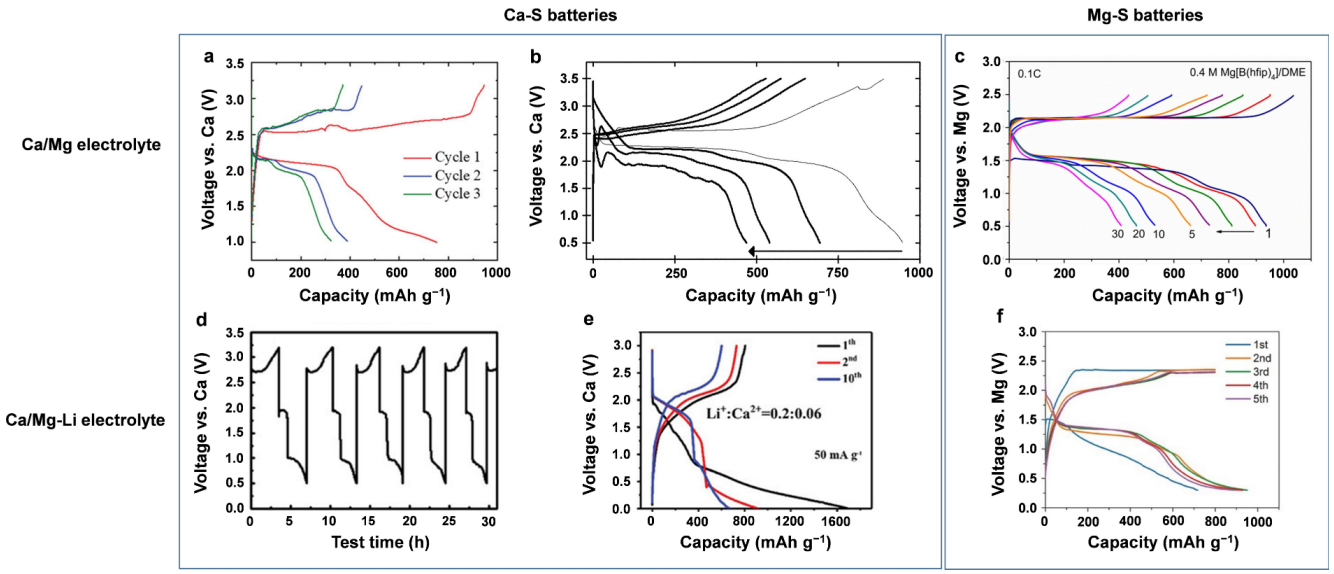

Figure 13. Voltage profiles of Ca S and Mg S batteries applying single-cation electrolytes: (a) KB/S cathode and (b) ACC/S cathode in $Ca[B(hfip)_4]_2$/DME (C/10), (c) ACC/S cathode in $Mg[B(hfip)_4]_2$/DME (C/10); as well as hybrid electrolytes utilizing an additional Li salt: (d) CNF/S cathode in 0.5 M $LiCF_3SO_3$ + 0.2 M $Ca(CF_3SO_3)_2$/G4 (C/10), (e) S@C NS cathode in 0.2 M $LiPF_6$ + 0.06 M $Ca(BF_4)_2$/EC-EMC-DMC (C/33) and (f) ZIF C-S cathode in LiTFSI + $(HMDS)_2Mg$-$AlCl_3$/G2 (C/10). Reproduced with permissions. (a) Copyright 2020, the Authors, published by Wiley.[127] (b) Copyright 2020, American Chemistry Society.[129] (c) Copyright 2018, American Chemistry Society.[130] (d) Copyright 2019, Wiley.[131] (e) Copyright 2024, Wiley.[132] (f) Copyright 2018, Wiley.[133] Following the success of weakly coordinating anions, namely the $Mg[B(hfip)_4]_2$ electrolyte for Mg S cells,[130] $Ca[B(hfip)_4]_2$/DME was applied by Li et al. in subsequent studies enabling reversible sulfur redox reactions for the first time in pure calcium electrolyte.[127] In a parallel work, Scafuri et al. investigated the electrochemical mechanism via XPS and operando Ca and S K-edge XANES revealing the classical pathway of metal-sulfur batteries including soluble polysulfides as well as solid CaS and S_8 at the end of discharge and charge, respectively.[129]

due to the thermodynamic value of Li–S being higher (2.20 V).

However, the Li mediator is beneficial by forming $Ca_xLi_yS_n$ instead of the metal sulfide (CaS, MgS) resulting in a facilitated re-oxidation and reduced charge overpotentials. In that context, caution has to be paid if comparing distinct capacity values and decays in Ca–S cells as the reported discharge cut-off voltages significantly vary from 1 V to 0.5 V and even 0 V (Figure 13a,b,d,e). Thus, CaS might only partially be formed, which consequently diminishes the capacity gain, but might enhance the reversibility, i.e. cycling stability. However, in either case, the capacity decay is huge dropping from $>800\,mAh\,g^{-1}$ to $<200\,mAh\,g^{-1}$ after 15–20 cycles.[127,129,131] This might be originated in the higher solubility of lithium polysulfides compared to calcium (and magnesium) polysulfides[134] and a consequent loss of active material.

Like in all metal-sulfur batteries, the loss can be counteracted by popular sulfur retention approaches like the sulfur incorporation in a carbon matrix. The sulfur hosts yet applied in the Ca–S system comprise Ketjenblack (KB),[127] ACC[127,129] and CNF[131] – achieving hardly no retention effect. In a recent approach, Wu et al. therefore pursued a carbon layer confined small-molecule/covalent sulfur composite nanosheet (S@C NS, >60 wt % S), in which the formation of soluble polysulfides is mostly inhibited.[132] The S@C NS was synthesized by a one-step co-deposition process of C and S from CS_2 in a plasma-enhanced CVD process at 300 °C mostly forming covalent –C–S–C– bonds and small molecules (S_2–S_6, 0.4–0.5 nm) (Figure 14). By latter incorporation, the carbon layer space is enlarged to 0.38–0.46 nm, which enhances the Ca^{2+} diffusion. However, the stated solid-solid sulfur conversion to CaS/Li_2S is only possible applying a hybrid electrolyte of $LiPF_6$ and $Ca(BF_4)_2$. Note that, PF_6^- and BF_4^- can only be applied due to the confined sulfur which prevents their nucleophilic reaction with the sulfur species. The superior cycling stability therein is further assigned to Li contributing to both, the SEI and CEI formation comprising LiF, $LiPO_xF_y$ and Li_xPF_y which exhibit higher ion conductivity than pure CaF_2. Further, the applied electrolyte solvent (EC/EMC/DMC) is known from Li–S research to be prone for decomposition and SEI/CEI formation. Interestingly, Ca salts were also applied vice versa in a hybrid electrolyte for Na–S cells ($Ca(PF_6)_2$ + $NaPF_6$ in PC/FEC) by Zhou et al. wherein Ca suppresses the Na dendrite growth at the anode.[135]

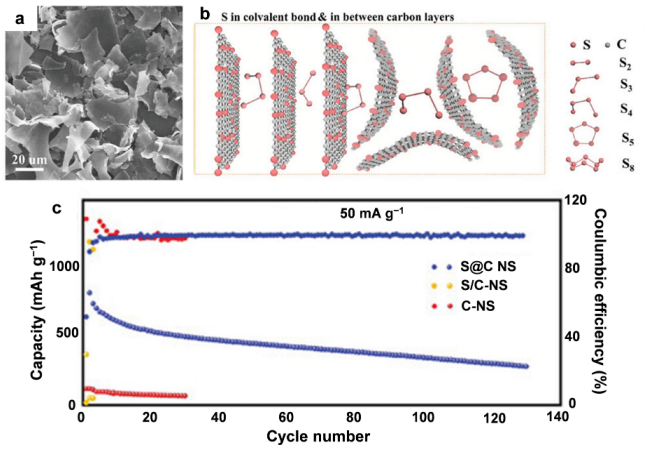

Figure 14. Sulfur confined carbon nanosheet enable long-lasting Ca S batteries with hybrid $LiPF_6 + Ca(BF_4)_2$ electrolyte. Reproduced with permission.[132] Copyright 2024, Wiley.

7.2. Selenium Redox

Elemental selenium represents another popular conversion material to be combined with metal anodes. In contrast to sulfur being an insulator, selenium offers sufficient electronic conductivity ($1\times10^{-3}\,S\,m^{-1}$ vs $5\times10^{-28}\,S\,m^{-1}$ for S) to require less conductive additives while also providing a high volumetric yet lower specific capacity ($3265\,mAh\,cm^{-3}$ and $680\,mAh\,g^{-1}$, respectively) compared to sulfur.

The first Ca–Se battery was lately reported by Zhou et al.[136] in 2022. By utilizing 0.25 M $Ca(TFSI)_2$ in EC/DMC, activated carbon as anode, a highly-ordered CMK-3 as host for Se melt infiltration and a CNT interlayer in between cathode and separator to mitigate the polyselenide shuttle, the Ca–Se cell delivered $150\,mAh\,g^{-1}$ after 300 cycles at a rather high current density of $500\,mA\,g^{-1}$ (0.74 C) (Figure 15b, c). This demonstrates that the di-valence and large size of Ca^{2+} (114 pm vs. 86 pm and 90 pm for Mg^{2+} and Li^+, respectively) is not an obstacle for designing high-power RCBs[136] – which is in contrast to rechargeable Mg battery (RMB) cells wherein an attractive rate performance is difficult to achieve due to the high charge density of Mg^{2+}.

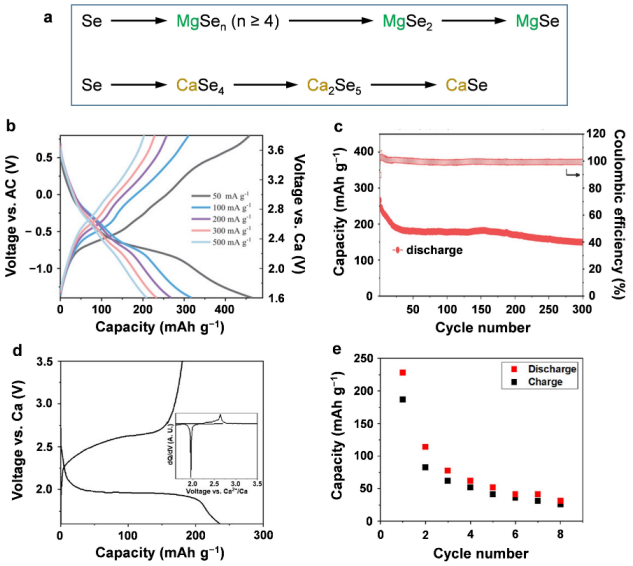

Figure 15. (a) Proposed reaction pathway of Ca Se in comparison to Mg Se system.[136] (b–e) Voltage profile and cycling stability of Ca Se cells comprising a (b,c) AC anode, Se/CMK3 cathode, CNT interlayer and 0.25 M $Ca(TFSI)_2$ in EC/DMC at $500\,mA\,g^{-1}$ (0.74C). and (d,e) Ca anode, Se/AC cathode and 0.2 M $Ca[B(hfip)_4]_2$/DME at $100\,mA\,g^{-1}$. Reproduced with permission. (b) and (c) Copyright 2022, Wiley.[136] (d) and (e) Copyright 2023, the Authors, published by American Chemistry Society.[138]

Nevertheless, the theoretically predicted multi-step reaction pathway is similar to the Mg–Se system,[137] following a transformation from Se to the triclinic $CaSe_4$, orthorhombic Ca_2Se_5 and finally to the cubic CaSe (Figure 15a).

$$Ca + Se \leftrightarrow CaSe \ (Q_{theo} = 680\,mAh\,g^{-1},\ U_{theo} = 2.26\,V)$$

Yet, the reaction is further reported to be incomplete (only 0.7 Ca^{2+} per Se at the discharge cut-off), which is in line with the still slopy profile at the discharge cut-off voltage. As the Se cathode shows superior reversibility at high rates, it is concluded that the reversibility of the Ca metal anode is the bottleneck towards high-energy Ca–Se battery. Another approach was reported by Kim et al. applying a similar cell setup comprising a Se melt-infiltrated activated carbon (1:1 wt.), 0.2 M $Ca[B(hfip)_4]_2$/DME electrolyte and glass fiber separator – yet applying calcium metal instead of an AC anode.[138] In contrast to the previous results, poor cycling stability and a single-plateau voltage profile was observed (Figure 15d, e).

The poor performance was only generally attributed to either cathode (dissolution and pulverization) or anode issues (surface passivation) – or both. As the electrolyte allows reversible Ca stripping/plating and no Se compounds were detected post mortem on the Ca surface (i.e. absence of the polyselenide shuttle), a (sole) anode issue is unlikely. Due to the similar cathode composition, it is supposed to be originated in the electrolyte-cathode interactions – either due to steric hindrance of the anion in the carbon microstructure ($TFSI^-$ vs. $[B(hfip)_4]^-$) or the solvent incompatibility (EC/DMC vs. DME). Latter is likely as the solvent mainly determines the dissolution behaviour and therefore kinetics.[134,139] Further, carbonates are known to contribute to a CEI, which might encapsulate the selenium species.

7.3. Other Conversion Compounds

Apart from sulfur and selenium, other elemental redox chemistries including oxygen and chlorine were recently reported to show reversibility in calcium cells. Although oxygen (air) cathode provides a high theoretical capacity/energy, the reversibility of O_2 redox in the presence of Ca^{2+} is rather poor. This is due to the fact that fully discharged product CaO is both ionically and electronically insulating, but also originated from the strong bonding energy of Ca–O that impedes the re-oxidation to form O_2, similar to the case of Mg-O_2 system.[16,140] To facilitate the decomposition of CaO, Shiga et al. introduced 2,2,6,6-tetramethylpiperidine 1-oxyl (TEMPO)–anion complex as catalyst, which enables partially re-oxidation of the discharged products.[141] Very recently, Ye et al. proposed a two-electron redox of CaO_2/O_2, which bypasses the formation of CaO as the discharged product. To couple the O_2 cathode with a Ca metal anode, an ionic liquid electrolyte was developed, comprising Ca-$(TFSI)_2$ in the blend of 1-ethyl-3-methylimidazolium tetrafluoroborate (EMIM-BF_4) and dimethyl sulfoxide (DMSO). The prototype Ca-O_2 battery exhibited stable cycling at 1 $A\,g^{-1}$ for 700 cycles, providing a capacity of ~500 $mAh\,g^{-1}$.[142]

Rechargeable Ca-Cl_2 batteries normally apply $SOCl_2$ as both the electrochemically active material and the solvent of electrolyte, thereby also termed Ca-$SOCl_2$ batteries.[143] Pioneering work on the Ca-$SOCl_2$ system indicated severe passivation of the metal anode by $CaCl_2$, which was formed mainly by chemical reaction between Ca metal and $SOCl_2$.[144] As a result, only primary Ca-$SOCl_2$ cells were developed. Reversible $CaCl_2$/Cl_2 redox can be achieved by using lithium difluoro(oxalate)borate (LiDFOB) as a mediator. A recent study indicated that the B–F and C=O functional groups in LiDFOB could promote the dissociation of $CaCl_2$ and the migration of the resultant species. In addition, the mediator also inhibited the passivation of Ca anode by adsorbing $DFOB^-$ on its surface. Therefore, the Ca-Cl_2 battery provided a discharge voltage of ~3 V and could be cycled at 200 $mAh\,g^{-1}$ for 100 cycles. Interestingly, no significant volume change was observed in the pouch cell after cycling, despite of the Cl_2 generation, which might be adsorbed within the graphite cathode.[145] In contrast to Ca-$SOCl_2$ system, rechargeable Mg-$SOCl_2$ battery is still not reported.[146] The difference might again hint at a faster reaction kinetics of the Ca chemistry.

Besides the elemental cathodes, transition metal sulfides (TMSs) were also investigated for the storage of Ca^{2+}. CuS is a conversion material being attractive due to its high specific capacity and sufficient electronic conductivity while being environmentally friendly. Ren et al. applied a CuS-nanocage/acetylene black composite cathode in several cation systems (Ca, Mg, Zn, Fe, Al) to compare their performance.[147] The pathway for the Ca redox follows the formation of Cu_2S to finally Cu and CaS.

$$2\ CuS + Ca^{2+} + 2\ e^- \leftrightarrow Cu_2S + CaS$$
$$Cu_2S + Ca^{2+} + 2\ e^- \leftrightarrow 2\ Cu + CaS\ (Q_{theo} = 560\,mAh\,g^{-1})$$

By applying a $Ca(TFSI)_2$ in EC/DMC/PC/EMC (2:3:2:3) electrolyte and an AC anode, a high capacity of 492 $mAh\,g^{-1}$ in the first discharge and 100 $mAh\,g^{-1}$ after 30 cycles at 100 $mA\,g^{-1}$ are achieved (Figure 16a). Analogous to Mg, the re-oxidation to CuS during charge only occurs partially, resulting in the significant initial capacity loss. Considering the number of intermediate phases, Kisu et al.[35] found that Ca^{2+} (114 pm) follows the reaction mechanism of Na (116 pm) with a multistep profile rather than Mg^{2+} (86 pm) and Li^+ (90 pm) with a two-step profile. It is concluded that the reaction mechanism strongly depends on the cation size – with the larger cation inducing a lattice strain which leads to the formation of a thermodynamically unfavourable phase. By applying $Ca(CB_{11}H_{12})_2$ in DME/THF an excellent rate capability at up to 3000 $mA\,g^{-1}$ (5.4C) (Figure 16b) and long-term cycling stability at 1000 $mA\,g^{-1}$ (1.8C) (Figure 16c) is achieved. Remarkably, Ca metal was applied as counter electrode (in a three-electrode setup) while previous studies of other conversion cathodes (see above) only achieved similar cycle numbers utilizing an AC counter electrode.

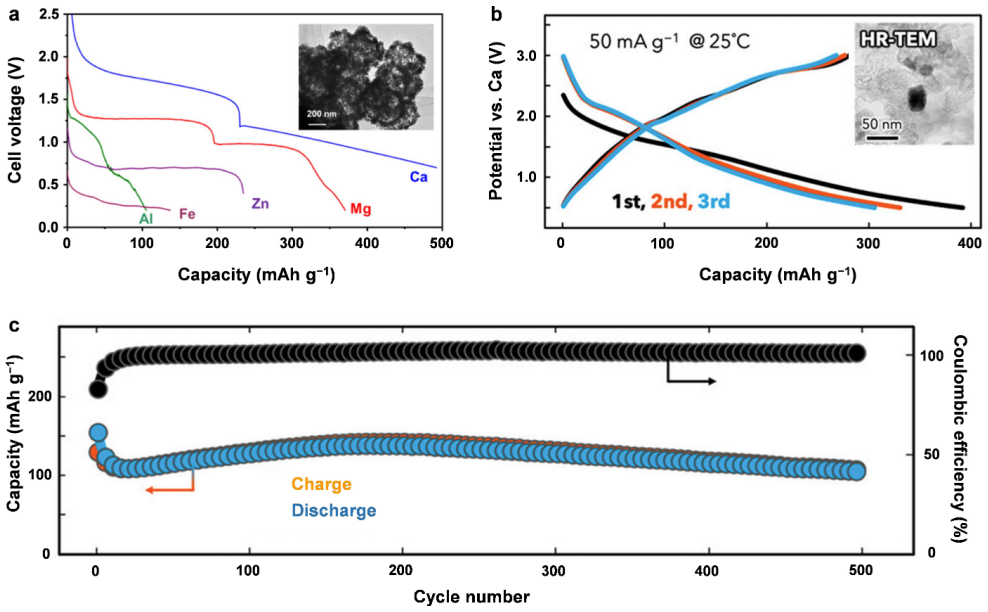

Figure 16. (a) Comparison of metal-CuS systems in terms of cell voltage and capacity gain. Reproduced with permission.[147] Copyright 2023, Wiley. The Ca cells comprised an ACC anode and 0.8 M $Ca(TFSI)_2$ in EC/DMC/PC/EMC (2:3:2:3) electrolyte, (b) Rate capability and (c) cycling stability of CuS in $Ca(CB_{11}H_{12})_2$ in DME/THF. Reproduced with permission.[35] Copyright 2023, the Authors, published by Wiley.

Among TMSs, pyrite FeS_2 has emerged as a promising cathode material for metal ion batteries.[148] So far, only few groups have investigated the potential of FeS_2 conversion cathode for Ca and Mg batteries inspired by the previous application of this cathode for Li and Na. The preliminary investigations revealed the lack of reversible conversion of FeS_2 in the Ca and Mg system when using single-salt electrolytes. The application of hybrid electrolyte based on Ca/Mg- accompanied with a Li-salt have ensured favorable Li-driven conversion of FeS_2. Meng et al. reported that FeS_2 in combination with a Ca metal anode while using dual-salt ($Ca(BH_4)_2$+$LiBH_4$/THF) electrolyte exhibits a high discharge capacity of 303 mAh g^{-1} with a CE of 96.7 % over 200 cycles.[148c] The authors emphasized that not only the advantageous Li-driven conversion of FeS_2, but also the improved desolvation kinetics of Ca^{2+} ions lead to reversibility with suppressed overpotential at the Ca anode throughout the cycle. As a comparison with the Mg system, Zhang et al. have explored the ability of dual metal battery concept (Mg and Li) in employing the FeS_2 cathode reversibly.[149] Hereby the metal Li at the anode is substituted by Mg while using dual-salt electrolytes with adjustable concentration of Mg^{2+} and Li^+. The study has reported a maximum reversible capacity of 600 mAh g^{-1} depending on the concentration of Li salts in the hybrid electrolytes.

Vanadium tetrasulfide (VS_4) is another compound of the TMS family. Li et al. investigated VS_4 as a cathode material for rechargeable Mg and Ca batteries using the respective fluorinated alkoxyborate electrolytes.[54] Their study concludes that the electrochemical storage of Mg^{2+} ions in the VS_4 cathode material follows an insertion mechanism, however, with the reversible formation/dissociation of the S–S bonds in the VS_4 backbones. As the VS_4 cathode delivered a similar capacity at comparable potentials in Ca batteries, a similar storage mechanism was proposed, but remains to be experimentally validated.

8. Summary & Outlook

Recently, EU has adopted new rules on batteries, where a compulsory carbon footprint declaration is required for EVs. This regulation marks the urgent need to strategically shift towards more sustainable battery chemistries. In this background, research development in RCBs has attracted increasing interest. Due to the technological advantages of Ca-based batteries, major scientific breakthroughs of the system might ultimately lead to transformative innovations in the battery field.

To achieve viable Ca batteries, non-aqueous electrolyte with high oxidative stability, in which Ca can be plated and stripped efficiently, is still a core task for the community. In light of the development of Mg electrolyte, Ca analogue compounds, mainly $Ca(BH_4)_2$ and calcium fluorinated alkoxyborate/-aluminate were developed and intensively investigated. However, none of them enables a high Coulombic efficiency of Ca metal anode, and at the same time provides a large electrochemical window, which marks significant difference of electrolyte chemistry between Mg and Ca. First of all, Ca is chemically more active than Mg, which makes it more challenging to achieve high CE while maintaining a clean metal surface. Worse is that, Ca^{2+} does not form complex ion clusters with Cl^-, which hinders the transfer of knowledge from Cl-based Mg electrolytes. In fact, all of the developed Ca electrolytes decompose partially on the metal surface, which calls for further molecular design of the anions that are stable against Ca anode, or promote the formation of an SEI. In addition to the electrolyte com-

pounds, the choice of solvent also determines the plating/stripping efficiency of Ca. Ca^{2+} has a lower charge density than Mg^{2+}, therefore weaker interaction with polar solvent. However, it prefers a higher coordination number of 6–8 due to its large ionic size,[150] attributing to a higher solvation energy than Mg^{2+} (Figure 3b). In this regard, applying solvent or solvent blend with a weak chelating capability would lead to a weak coordination structure that facilitate desolvation.[151] In fact, electrochemical reduction of strongly solvated Ca^{2+} (e.g. with longer-chain glymes)[30a] may lead to partial solvent decomposition that generates electrochemically inactive species, which impede further plating/stripping process.[152] However, if those side reactions result in the formation of SEI, reversible Ca^{2+}/Ca^{0} redox can be still achieved.[37,153] To this end, a more comprehensive understanding of the plating/stripping reactions and the interfacial transport mechanisms (in the abovementioned electrolyte systems) would be of great beneficial for a dedicated design of the solvation structure of Ca^{2+} with desired anion-solvent couple.

A stable anode reaction could be also achieved by applying alternative anodes that are chemically more inert than metallic Ca. Alloy anodes particularly Ca–Sn alloys were recently discovered to show excellent cyclability in a variety of electrolytes. As already demonstrated in Mg batteries, other p-block metals such as Bi, Sb etc. deserve further investigation in Ca batteries. However, de-/calciation of alloys generally undergo complicated reaction mechanisms with the formation of various intermediates that provide different redox potentials and exhibits different kinetic behaviors. This calls for further mechanistic investigations to clarify the electrochemically active compositions, and based on which developing strategies to allow deeper de-/calciation. On the other hand, alloy anodes are still only used for the evaluation of organic cathodes. Their capability to couple with inorganic cathodes awaits experimental validation.

In addition to metal deposition and alloy formation, intercalation reaction is another key topic for Ca-based batteries. While bare Ca^{2+} intercalation generally suffers from sluggish diffusion kinetics in rigid crystal lattice, solvent co-intercalation approach employs solvated Ca^{2+} as the intercalant and thereby enhancing ion mobility by shielding the double charge of Ca^{2+}. The co-intercalation strategy enables graphite anode to reversibly host Ca^{2+} at a high current rate. Inspiringly, improvement of Ca storage in layered oxide cathodes was also evident by water co-intercalation or applying water as structural pillar (hydrated oxides). In particular, the hydrated layered oxides demonstrated reversible Ca^{2+} storage and promising cycling stability, which calls for further evaluation of these materials against Ca metal anodes. To further exploit the advantage of co-intercalation approach, organic solvent with large electrochemical window, and structural flexibility should be investigated. This field was pioneered by Wang et al. with the development of methoxyethylamine, and could be a promising direction for future studies. As for the downside, co-intercalation chemistry is normally based on strong chelating solvent, which induces a high kinetic barrier for desolvation at the counter electrode. Possible solutions to this issue include: (1) to build a co-intercalation battery that employs cathode and anode both based on co-intercalation mechanism; (2) to design proper electrolyte that allows co-intercalation at the cathode side, and promotes SEI formation at the Ca anode; (3) to develop novel co-intercalation chemistries beyond solvent co-intercalation.

Targeting the sluggish diffusion kinetics of Ca^{2+}, insertion cathode hosts should also be properly designed. In particular, the size effect of the guest cation should be taken into account seriously. Due to the similar ionic radius between Ca^{2+} and Na^{+}, PBAs and NASICON compounds were evaluated and exhibited fair reversibility for Ca^{2+} de-/insertion. The successful demonstration also motivates to evaluate other Na^{+} hosts with large vacancies as cathode materials for Ca batteries.[13,44] Furthermore, the increased ionic radius also varies the occupation preference in layered compounds from octahedral to prismatic coordination. Again similar to the case of Na^{+} insertion, where prismatic coordination reduces the repulsion between neighbouring guest cations. In fact, theoretical investigations already predicted some p-type oxides with low diffusion barrier, which deserve further experimental validation. On the other hand, till now, most of the cathodes were investigated in model cell configurations applying capacitive carbon counter electrode and electrolyte that is incompatible with Ca metal anode. Some efforts were made to evaluate the developed materials against Ca metal anode, but mostly with much inferior performance. This may be due to the passivation of metal anode that impedes further electrochemical reactions, but also indicates energy-intensive Ca^{2+} desolvation at cathode as another possible reason. The influence of electrolyte particular the solvation structure of Ca^{2+} on its insertion into cathode host requires further investigation. The situation also calls for the development of reliable cell configuration for the cathode evaluation, fare comparison of the performance from different studies, and the construction of full-cell Ca batteries.

Beyond intercalation, other storage mechanisms such as conversion reactions or coordination chemistries exhibit more promising results. In contrast to the sluggish Ca^{2+} mobility in rigid inorganic host lattice, organic cathodes are capable of reversibly hosting Ca^{2+} at much higher C-rates, due to their molecular flexibility and fast redox reactions. As the redox centers are easier accessible by various charge carriers, organic compounds developed for other cell chemistries could in principle also viable for Ca batteries. Of course, there are other issues associated with Ca^{2+}, e.g. its strong solvation structure and ion-pairing effect, which lowers the utilization of active material and swelling of the cathode. Nevertheless, the kinetic advantage makes it easier to transfer knowledge from other batteries to Ca systems. As the flipside of the organic cathode, their performance relies on large amount of carbon, due to the low electronic conductivity. Tackling this issue, conjugated framework structures such as COFs or MOFs can be a feasible way.[126a] Furthermore, organic compounds have lower density, which reduces the volumetric energy density. While this issue could be alleviated by coupling with a metal anode, the organic

cathode might be more suitable for applications where volumetric parameters are not critically required.

In a similar manner, conversion materials have great potential as cathode for Ca-based batteries due to their high capacity and less restricted rate capability compared to Mg batteries. The proof-of-concept studies demonstrated Ca–S and Ca–Se chemistries with fairly good reversibility. However, realizing a high-energy Ca-chalcogen battery still needs to address the strong bonding of Ca–S (or Ca–Se) and the passivation or Ca metal anode. Analogous to the Mg–S system, organosulfurs like SPAN or polar solvents like DMSO are of interested to enhance the cycling stability and sulfur utilization, respectively. Generally, the electrolyte selection is key with pure Ca electrolytes being superior to hybrid approaches due to the non-limited ion reservoir. Among the weakly-coordinating anions, $[B(hfip)_4]^-$ and $CB_{11}H_{12}^-$ are promising – regarding solvents, carbonates can play a crucial role in SEI and CEI formation. Other elemental cathodes (e.g. O_2 and Cl_2) have just demonstrated their reversible redox in the presence of Ca^{2+}. While promising, more efforts should be made for the investigation on the respective systems.

All in all, Ca chemistry is still largely unexplored, which leaves a number of fundamental challenges to be addressed, but also offers potential pathways to obtain greener batteries with high energy density. At the current stage, it is difficult to evaluate the potential application scenario of Ca-based batteries, as viable Ca chemistries are still to be developed. However, the use of Ca^{2+} as charge carriers renders the sustainability of the technology, and further discovery of the electrode materials based on abundant elements would enhance this advantage. In this sense, Ca battery could find its place in the battery market, if progressive development can be achieved.

Acknowledgements

This work is financially supported by the National Natural Science Foundation of China with grant No 52002350, Science Fund Program of Shandong Province, and Taishan Scholars of Shandong Province. It was partially funded by the Federal Ministry of Education and Research (Bundesministerium für Bildung und Forschung, BMBF) of Germany within the project "CaSino" (03XP0487F) and the German Research Foundation (DFG) under Project ID 390874152 (POLiS Cluster of Excellence). This work contributes to the research performed at CELEST (Center for Electrochemical Energy Storage Ulm-Karlsruhe). Z. Li and S. Cui contribute equally to this work.

Conflict of Interest

The authors declare no conflict of interest.

Data Availability Statement

Data sharing is not applicable to this article as no new data were created or analyzed in this study.

Keywords: Calcium battery · Calcium electrolyte · Ca^{2+} intercalation · Conversion cathode · Alloy anode

[1] M. Maisch, *pv magazine* **2023**.
[2] P. Greim, A. A. Solomon, C. Breyer, *Nat. Commun.* **2020**, *11*, 4570.
[3] G. Y. Gene Berdichevsky, *Sila Nanotechnologies Inc.* **2020**.
[4] a) I. D. Hosein, *ACS Energy Lett.* **2021**, *6*, 1560–1565; b) L. Stievano, I. de Meatza, J. Bitenc, C. Cavallo, S. Brutti, M. A. Navarra, *J. Power Sources* **2021**, *482*, 228875.
[5] A. Ponrouch, M. R. Palacin, *Curr. Opin. Electrochem.* **2018**, *9*, 1–7.
[6] S. M. Selis, J. P. Wondowski, R. F. Justus, *J. Electrochem. Soc.* **1964**, *111*, 6–13.
[7] D. Aurbach, R. Skaletsky, Y. Gofer, *J. Electrochem. Soc.* **1991**, *138*, 3536.
[8] A. Ponrouch, C. Frontera, F. Barde, M. R. Palacin, *Nat. Mater.* **2016**, *15*, 169–172.
[9] D. Wang, X. Gao, Y. Chen, L. Jin, C. Kuss, P. G. Bruce, *Nat. Mater.* **2018**, *17*, 16–20.
[10] a) Z. Li, O. Fuhr, M. Fichtner, Z. Zhao-Karger, *Energy Environ. Sci.* **2019**, *12*, 3496–3501; b) A. Shyamsunder, L. E. Blanc, A. Assoud, L. F. Nazar, *ACS Energy Lett.* **2019**, *4*, 2271–2276.
[11] a) J. Park, Z. L. Xu, G. Yoon, S. K. Park, J. Wang, H. Hyun, H. Park, J. Lim, Y. J. Ko, Y. S. Yun, K. Kang, *Adv. Mater.* **2020**, *32*, e1904411; b) S. J. Richard Prabakar, A. B. Ikhe, W. B. Park, K. C. Chung, H. Park, K. J. Kim, D. Ahn, J. S. Kwak, K. S. Sohn, M. Pyo, *Adv. Sci.* **2019**, *6*, 1902129.
[12] a) M. Wang, C. Jiang, S. Zhang, X. Song, Y. Tang, H. M. Cheng, *Nat. Chem.* **2018**, *10*, 667–672; b) Z. Zhao-Karger, Y. Xiu, Z. Li, A. Reupert, T. Smok, M. Fichtner, *Nat. Commun.* **2022**, *13*, 3849.
[13] a) S. Kim, L. Yin, M. H. Lee, P. Parajuli, L. Blanc, T. T. Fister, H. Park, B. J. Kwon, B. J. Ingram, P. Zapol, R. F. Klie, K. Kang, L. F. Nazar, S. H. Lapidus, J. T. Vaughey, *ACS Energy Lett.* **2020**, *5*, 3203–3211; b) Z. L. Xu, J. Park, J. Wang, H. Moon, G. Yoon, J. Lim, Y. J. Ko, S. P. Cho, S. Y. Lee, K. Kang, *Nat. Commun.* **2021**, *12*, 3369.
[14] Y. Tian, G. Zeng, A. Rutt, T. Shi, H. Kim, J. Wang, J. Koettgen, Y. Sun, B. Ouyang, T. Chen, Z. Lun, Z. Rong, K. Persson, G. Ceder, *Chem. Rev.* **2021**, *121*, 1623–1669.
[15] a) J. D. Forero-Saboya, E. Marchante, R. B. Araujo, D. Monti, P. Johansson, A. Ponrouch, *J Phys Chem C Nanomater Interfaces* **2019**, *123*, 29524–29532; b) J. D. Forero-Saboya, D. S. Tchitchekova, P. Johansson, M. R. Palacín, A. Ponrouch, *Adv. Mater. Interfaces* **2021**, *9*, 2101578.
[16] M. E. Arroyo-de Dompablo, A. Ponrouch, P. Johansson, M. R. Palacin, *Chem. Rev.* **2020**, *120*, 6331–6357.
[17] M. D. Radin, A. Van der Ven, *Chem. Mater.* **2016**, *28*, 7898–7904.
[18] R. Shannon, *Acta Crystallogr. Sect. A* **1976**, *32*, 751–767.
[19] a) M. Shakourian-Fard, G. Kamath, K. Smith, H. Xiong, S. K. R. S. Sankaranarayanan, *J. Phys. Chem. C* **2015**, *119*, 22747–22759; b) M. Shakourian-Fard, G. Kamath, S. K. Sankaranarayanan, *ChemPhysChem* **2016**, *17*, 2916–2930; c) M. Shakourian-Fard, G. Kamath, S. K. Sankaranarayanan, *ChemPhysChem* **2015**, *16*, 3607–3617.
[20] M. Shakourian-Fard, G. Kamath, S. M. Taimoory, J. F. Trant, *J. Phys. Chem. C* **2019**, *123*, 15885–15896.

[21] D. Wang, X. Gao, Y. Chen, L. Jin, C. Kuss, P. G. Bruce, *Nat. Mater.* **2018**, *17*, 16–20.

[22] K. Ta, R. Zhang, M. Shin, R. T. Rooney, E. K. Neumann, A. A. Gewirth, *ACS Appl. Mater. Interfaces* **2019**, *11*, 21536–21542.

[23] M. Paskevicius, B. Richter, M. Polański, S. P. Thompson, T. R. Jensen, *Dalton Trans.* **2016**, *45*, 639–645.

[24] Y. Jie, Y. Tan, L. Li, Y. Han, S. Xu, Z. Zhao, R. Cao, X. Ren, F. Huang, Z. Lei, G. Tao, G. Zhang, S. Jiao, *Angew. Chem. Int. Ed. Engl.* **2020**, *59*, 12689–12693.

[25] S. A. McClary, D. M. Long, A. Sanz-Matias, P. G. Kotula, D. Prendergast, K. L. Jungjohann, K. R. Zavadil, *ACS Energy Lett.* **2022**, *7*, 2792–2800.

[26] Z. Yang, N. J. Leon, C. Liao, B. J. Ingram, L. Trahey, *ACS Appl. Mater. Interfaces* **2023**, *15*, 25018–25028.

[27] Z. Zhao-Karger, M. E. Gil Bardaji, O. Fuhr, M. Fichtner, *J. Mater. Chem. A* **2017**, *5*, 10815–10820.

[28] S. Y. Li, J. H. Zhang, S. C. Zhang, Q. L. Liu, H. Cheng, L. Fan, W. D. Zhang, X. Y. Wang, Q. Wu, Y. Y. Lu, *Nat. Energy* **2024**, *9*, 285–297.

[29] J. Forero-Saboya, C. Davoisne, R. Dedryvère, I. Yousef, P. Canepa, A. Ponrouch, *Energy Environ. Sci.* **2020**, *13*, 3423–3431.

[30] a) N. T. Hahn, D. M. Driscoll, Z. Yu, G. E. Sterbinsky, L. Cheng, M. Balasubramanian, K. R. Zavadil, *ACS Appl. Energ. Mater.* **2020**, *3*, 8437–8447; b) D. M. Driscoll, N. K. Dandu, N. T. Hahn, T. J. Seguin, K. A. Persson, K. R. Zavadil, L. A. Curtiss, M. Balasubramanian, *J. Electrochem. Soc.* **2020**, *167*, 160512.

[31] L. H. B. Nguyen, J.-S. Filhol, *Adv. Energy Mater.* **2023**, *13*, 2300311.

[32] K. V. Nielson, J. Luo, T. L. Liu, *Batteries & Supercaps* **2020**, *3*, 766–772.

[33] a) X. Xie, N. J. Leon, D. W. Small, E. W. C. Spotte-Smith, C. Liao, K. A. Persson, *J. Phys. Chem. C* **2022**, *126*, 20773–20785; b) T. Pavcnik, J. D. Forero-Saboya, A. Ponrouch, A. Robba, R. Dominko, J. Bitenc, *J Mater Chem A Mater* **2023**, *11*, 14738–14747.

[34] K. Kisu, S. Kim, T. Shinohara, K. Zhao, A. Züttel, S.-i. Orimo, *Sci. Rep.* **2021**, *11*, 7563.

[35] K. Kisu, R. Mohtadi, S. I. Orimo, *Adv. Sci.* **2023**, *10*, e2301178.

[36] C. Bodin, J. Forero Saboya, P. Jankowski, K. Radan, D. Foix, C. Courrèges, I. Yousef, R. Dedryvère, C. Davoisne, M. Lozinšek, A. Ponrouch, *Batteries & Supercaps* **2023**, *6*, e202200433.

[37] Z. Hou, R. Zhou, Y. Yao, Z. Min, Z. Lu, Y. Zhu, J. M. Tarascon, B. Zhang, *Angew. Chem. Int. Ed. Engl.* **2022**, *61*, e202214796.

[38] H. Lin, J. Meng, W. Guo, R. Li, Y. Yi, Y. Ma, C. F. Cheung, D. Aurbach, Z.-L. Xu, *Energy Environ. Sci.* **2024**, *17*, 6548–6558.

[39] a) M. Wang, W. Sun, K. Zhang, Z. Zhang, A. Du, S. Dong, J. Zhang, J. Liu, X. Chen, Z. Zhou, F. Li, Z. Li, G. Li, G. Cui, *Energy Environ. Sci.* **2024**, *17*, 630–641; b) J. Sun, J. Yan, F. Li, J. Li, J. Ma, G. Xu, P. Han, G. Hou, Y. Tang, S. Dong, J. Huang, G. Cui, *Adv. Mater.* **2024**, *36*, 2405384; c) B. Qin, Y. Ma, C. Li, H. Xu, J. Li, B. Xie, X. Du, S. Dong, G. Xu, G. Cui, *Energy Storage Mater.* **2023**, *61*, 102891.

[40] L. Wang, S. Riedel, Z. Zhao-Karger, *Advanced Energy Materials* **2024**, *n/a*, 2402157.

[41] X. Deng, L. Li, G. Zhang, X. Zhao, J. Hao, C. Han, B. Li, *Energy Storage Mater.* **2022**, *53*, 467–481.

[42] S. D. Pu, C. Gong, X. Gao, Z. Ning, S. Yang, J.-J. Marie, B. Liu, R. A. House, G. O. Hartley, J. Luo, P. G. Bruce, A. W. Robertson, *ACS Energy Lett.* **2020**, *5*, 2283–2290.

[43] A. Ponrouch, D. Tchitchekova, C. Frontera, F. Bardé, M. E. A.-d. Dompablo, M. R. Palacín, *Electrochem. Commun.* **2016**, *66*, 75–78.

[44] A. L. Lipson, B. Pan, S. H. Lapidus, C. Liao, J. T. Vaughey, B. J. Ingram, *Chem. Mater.* **2015**, *27*, 8442–8447.

[45] Z. Yao, V. I. Hegde, A. Aspuru-Guzik, C. Wolverton, *Adv. Energy Mater.* **2019**, *9*, 1802994.

[46] Y. Xiu, A. Mauri, S. Dinda, Y. Pramudya, Z. Ding, T. Diemant, A. Sarkar, L. Wang, Z. Li, W. Wenzel, M. Fichtner, Z. Zhao-Karger, *Angew. Chem. Int. Ed. Engl.* **2023**, *62*, e202212339.

[47] Z. Wang, Q. Su, J. Shi, H. Deng, G. Q. Yin, J. Guan, M. P. Wu, Y. L. Zhou, H. L. Lou, Y. Q. Fu, *ACS Appl. Mater. Interfaces* **2014**, *6*, 6786–6789.

[48] J. Niu, Z. Zhang, D. Aurbach, *Adv. Energy Mater.* **2020**, *10*, 2000697.

[49] S. J. Kim, J. Y. Park, Y. Shim, D. Chang, J. H. Chang, K. S. Dae, J. M. Yuk, *ACS Appl. Energ. Mater.* **2022**, *5*, 7944–7949.

[50] T. T. Tran, M. N. Obrovac, *J. Electrochem. Soc.* **2011**, *158*, A1411–A1416.

[51] W. J. Zhang, *J. Power Sources* **2011**, *196*, 13–24.

[52] R. Dominko, J. Bitenc, R. Berthelot, M. Gauthier, G. Pagot, V. Di Noto, *J. Power Sources* **2020**, *478*, 229027.

[53] A. Manthiram, *Nat. Commun.* **2020**, *11*, 1550.

[54] Z. Li, B. P. Vinayan, P. Jankowski, C. Njel, A. Roy, T. Vegge, J. Maibach, J. M. G. Lastra, M. Fichtner, Z. Zhao-Karger, *Angew. Chem. Int. Ed.* **2020**, *59*, 11483–11490.

[55] Y. Liang, H. Dong, D. Aurbach, Y. Yao, *Nat. Energy* **2020**, *5*, 646–656.

[56] C. Chen, F. Shi, Z.-L. Xu, *J. Mater. Chem. A* **2021**, *9*, 11908–11930.

[57] Y. Li, Y. Lu, P. Adelhelm, M. M. Titirici, Y. S. Hu, *Chem. Soc. Rev.* **2019**, *48*, 4655–4687.

[58] N. Emery, C. Hérold, P. Lagrange, *J. Solid State Chem.* **2005**, *178*, 2947–2952.

[59] W. Xu, M. M. Lerner, *Chem. Mater.* **2018**, *30*, 6930–6935.

[60] M. L. Divya, Y.-S. Lee, V. Aravindan, *ACS Energy Lett.* **2021**, *6*, 4228–4244.

[61] a) G. Yoon, H. Kim, I. Park, K. Kang, *Adv. Energy Mater.* **2016**, *7*, 1601519; b) B. Jache, P. Adelhelm, *Angew. Chem. Int. Ed. Engl.* **2014**, *53*, 10169–10173; c) D.-M. Kim, S. C. Jung, S. Ha, Y. Kim, Y. Park, J. H. Ryu, Y.-K. Han, K. T. Lee, *Chem. Mater.* **2018**, *30*, 3199–3203.

[62] Y. Yi, Y. Xing, H. Wang, Z. Zeng, Z. Sun, R. Li, H. Lin, Y. Ma, X. Pu, M. M. Li, K. Y. Park, Z. L. Xu, *Angew. Chem. Int. Ed. Engl.* **2024**, *63*, e202317177.

[63] A. K. Katz, J. P. Glusker, S. A. Beebe, C. W. Bock, *J. Am. Chem. Soc.* **1996**, *118*, 5752–5763.

[64] Z. Li, X. Mu, Z. Zhao-Karger, T. Diemant, R. J. Behm, C. Kubel, M. Fichtner, *Nat. Commun.* **2018**, *9*, 5115.

[65] G. Alvarez Ferrero, G. Åvall, K. A. Mazzio, Y. Son, K. Janßen, S. Risse, P. Adelhelm, *Adv. Energy Mater.* **2022**, *12*, 2202377.

[66] R. Verrelli, A. Black, R. Dugas, D. Tchitchekova, A. Ponrouch, M. R. Palacin, *J. Electrochem. Soc.* **2020**, *167*, 070532.

[67] D. S. Tchitchekova, A. Ponrouch, R. Verrelli, T. Broux, C. Frontera, A. Sorrentino, F. Bardé, N. Biskup, M. E. Arroyo-de Dompablo, M. R. Palacín, *Chem. Mater.* **2018**, *30*, 847–856.

[68] X. Sun, P. Bonnick, L. F. Nazar, *ACS Energy Lett.* **2016**, *1*, 297–301.

[69] Y. Murata, S. Takada, T. Obata, T. Tojo, R. Inada, Y. Sakurai, *Electrochim. Acta* **2019**, *294*, 210–216.

[70] N. Sa, H. Wang, D. L. Proffit, A. L. Lipson, B. Key, M. Liu, Z. Feng, T. T. Fister, Y. Ren, C.-J. Sun, J. T. Vaughey, P. A. Fenter, K. A. Persson, A. K. Burrell, *J. Power Sources* **2016**, *323*, 44–50.

[71] S. Gheytani, Y. Liang, F. Wu, Y. Jing, H. Dong, K. K. Rao, X. Chi, F. Fang, Y. Yao, *Adv. Sci.* **2017**, *4*, 1700465.

[72] R. Verrelli, A. P. Black, C. Pattanathummasid, D. S. Tchitchekova, A. Ponrouch, J. Oró-Solé, C. Frontera, F. Bardé, P. Rozier, M. R. Palacín, *J. Power Sources* **2018**, *407*, 162–172.

[73] J. Wang, S. Tan, F. Xiong, R. Yu, P. Wu, L. Cui, Q. An, *Chem. Commun.* **2020**, *56*, 3805–3808.

[74] M. S. Chae, H. H. Kwak, S.-T. Hong, *ACS Appl. Energ. Mater.* **2020**, *3*, 5107–5112.

[75] J. Wang, J. Wang, Y. Jiang, F. Xiong, S. Tan, F. Qiao, J. Chen, Q. An, L. Mai, *Adv. Funct. Mater.* **2022**, *32*, 2113030.

[76] X. Xu, M. Duan, Y. Yue, Q. Li, X. Zhang, L. Wu, P. Wu, B. Song, L. Mai, *ACS Energy Lett.* **2019**, *4*, 1328–1335.

[77] S. Hou, X. Ji, K. Gaskell, P.-f. Wang, L. Wang, J. Xu, R. Sun, O. Borodin, C. Wang, *Science* **2021**, *374*, 172–178.

[78] Z. Li, J. Häcker, M. Fichtner, Z. Zhao-Karger, *Adv. Energy Mater.* **2023**, *13*, 2300682.

[79] H. D. Yoo, Y. Liang, H. Dong, J. Lin, H. Wang, Y. Liu, L. Ma, T. Wu, Y. Li, Q. Ru, Y. Jing, Q. An, W. Zhou, J. Guo, J. Lu, S. T. Pantelides, X. Qian, Y. Yao, *Nat. Commun.* **2017**, *8*, 339.

[80] A. Roy, M. Sotoudeh, S. Dinda, Y. Tang, C. Kubel, A. Gross, Z. Zhao-Karger, M. Fichtner, Z. Li, *Nat. Commun.* **2024**, *15*, 492.

[81] L. E. Blanc, Y. Choi, A. Shyamsunder, B. Key, S. H. Lapidus, C. Li, L. Yin, X. Li, B. Gwalani, Y. Xiao, C. J. Bartel, G. Ceder, L. F. Nazar, *Chem. Mater.* **2022**, *35*, 468–481.

[82] a) G. G. Amatucci, F. Badway, A. Singhal, B. Beaudoin, G. Skandan, T. Bowmer, I. Plitza, N. Pereira, T. Chapman, R. Jaworski, *J. Electrochem. Soc.* **2001**, *148*, A940–A950; b) M. Hayashi, H. Arai, H. Ohtsuka, Y. Sakurai, *J. Power Sources* **2003**, *119*, 617–620; c) M. Bervas, L. C. Klein, G. G. Amatucci, *Solid State Ionics* **2005**, *176*, 2735–2747.

[83] a) T. Tojo, H. Tawa, N. Oshida, R. Inada, Y. Sakurai, *J. Electroanal. Chem.* **2018**, *825*, 51–56; b) M. Cabello, F. Nacimiento, R. Alcántara, P. Lavela, C. Pérez Vicente, J. L. Tirado, *Chem. Mater.* **2018**, *30*, 5853–5861.

[84] A. Roy, V. Bhagavathi Parambath, T. Diemant, G. Neusser, C. Kranz, R. J. Behm, Z. Li, Z. Zhao-Karger, M. Fichtner, *Batteries & Supercaps* **2022**, *5*, e202100305.

[85] Y. Xiong, Y. Lin, Q. Xue, *J. Electrochem. Soc.* **2020**, *167*, 160530.

[86] D. Maspoch, D. Ruiz-Molina, J. Veciana, *Chem. Soc. Rev.* **2007**, *36*, 770–818.

[87] Q. Liu, Z. Hu, M. Chen, C. Zou, H. Jin, S. Wang, S.-L. Chou, Y. Liu, S.-X. Dou, *Adv. Funct. Mater.* **2020**, *30*, 1909530.

[88] a) C. Chen, F. Shi, S. Zhang, Y. Su, Z. L. Xu, *Small* **2022**, *18*, e2107853; b) M. Cabello, F. Nacimiento, J. R. González, G. Ortiz, R. Alcántara, P. Lavela, C. Pérez-Vicente, J. L. Tirado, *Electrochem. Commun.* **2016**, *67*, 59–64; c) C. Zuo, F. Xiong, J. Wang, Y. An, L. Zhang, Q. An, *Adv. Funct. Mater.* **2022**, *32*, 2202975; d) A. P. Black, C. Frontera, A. Torres, M. Recio-Poo, P. Rozier, J. D. Forero-Saboya, F. Fauth, E. Urones-Garrote, M. E. Arroyo-de Dompablo, M. R. Palacín, *Energy Storage Mater.* **2022**, *47*, 354–364; e) B. Jeon, J. W. Heo, J. Hyoung, H. H. Kwak, D. M. Lee, S.-T. Hong, *Chem. Mater.* **2020**, *32*, 8772–8780; f) R. Li, Y. Lee, H. Lin, X. Che, X. Pu, Y. Yi, F. Chen, J. Yu, K. C. Chan, K. Y. Park, Z. L. Xu, *Adv. Energy Mater.* **2024**, *14*, 2302700.

[89] H. Park, C. J. Bartel, G. Ceder, P. Zapol, *Adv. Energy Mater.* **2021**, *11*, 2101698.

[90] H. Park, P. Zapol, *J. Mater. Chem. A* **2020**, *8*, 21700–21710.

[91] T. Hatakeyama, N. L. Okamoto, T. Ichitsubo, *J. Solid State Chem.* **2022**, *305*, 122683.

[92] B.-R. Chen, W. Sun, D. A. Kitchaev, J. S. Mangum, V. Thampy, L. M. Garten, D. S. Ginley, B. P. Gorman, K. H. Stone, G. Ceder, M. F. Toney, L. T. Schelhas, *Nat. Commun.* **2018**, *9*, 2553.

[93] H. Xia, X. Zhu, J. Liu, Q. Liu, S. Lan, Q. Zhang, X. Liu, J. K. Seo, T. Chen, L. Gu, Y. S. Meng, *Nat. Commun.* **2018**, *9*, 5100.

[94] T. R. Juran, J. Young, M. Smeu, *J. Phys. Chem. C* **2018**, *122*, 8788–8795.

[95] K. W. Nam, S. Kim, E. Yang, Y. Jung, E. Levi, D. Aurbach, J. W. Choi, *Chem. Mater.* **2015**, *27*, 3721–3725.

[96] M. Liu, Z. Rong, R. Malik, P. Canepa, A. Jain, G. Ceder, K. A. Persson, *Energy Environ. Sci.* **2015**, *8*, 964–974.

[97] M. E. A.-d. Dompablo, C. Krich, J. Nava-Avendaño, N. Biškup, M. R. Palacín, F. Bardé, *Chem. Mater.* **2016**, *28*, 6886–6893.

[98] W. Lu, J. Wang, G. Sai Gautam, P. Canepa, *Chem. Mater.* **2021**, *33*, 5809–5821.

[99] Y. You, X. L. Wu, Y. X. Yin, Y. G. Guo, *J. Mater. Chem. A* **2013**, *1*, 14061–14065.

[100] R. Y. Wang, C. D. Wessells, R. A. Huggins, Y. Cui, *Nano Lett.* **2013**, *13*, 5748–5752.

[101] F. Wang, X. Fan, T. Gao, W. Sun, Z. Ma, C. Yang, F. Han, K. Xu, C. Wang, *ACS Cent. Sci.* **2017**, *3*, 1121–1128.

[102] A. L. Lipson, S.-D. Han, S. Kim, B. Pan, N. Sa, C. Liao, T. T. Fister, A. K. Burrell, J. T. Vaughey, B. J. Ingram, *J. Power Sources* **2016**, *325*, 646–652.

[103] N. Kuperman, P. Padigi, G. Goncher, D. Evans, J. Thiebes, R. Solanki, *J. Power Sources* **2017**, *342*, 414–418.

[104] Q. Ni, Y. Bai, F. Wu, C. Wu, *Adv. Sci.* **2017**, *4*, 1600275.

[105] Y. Fang, J. Zhang, L. Xiao, X. Ai, Y. Cao, H. Yang, *Adv. Sci.* **2017**, *4*, 1600392.

[106] H. Li, M. Xu, Z. Zhang, Y. Lai, J. Ma, *Adv. Funct. Mater.* **2020**, *30*, 2000473.

[107] S. Chen, C. Wu, L. Shen, C. Zhu, Y. Huang, K. Xi, J. Maier, Y. Yu, *Adv. Mater.* **2017**, *29*, 1700431.

[108] Y.-U. Park, D.-H. Seo, H.-S. Kwon, B. Kim, J. Kim, H. Kim, I. Kim, H.-I. Yoo, K. Kang, *J. Am. Chem. Soc.* **2013**, *135*, 13870–13878.

[109] Y.-U. Park, D.-H. Seo, H. Kim, J. Kim, S. Lee, B. Kim, K. Kang, *Adv. Funct. Mater.* **2014**, *24*, 4603–4614.

[110] A. L. Lipson, S. Kim, B. Pan, C. Liao, T. T. Fister, B. J. Ingram, *J. Power Sources* **2017**, *369*, 133–137.

[111] J. Xie, Q. Zhang, *Small* **2019**, *15*, e1805061.

[112] T. Janoschka, M. D. Hager, U. S. Schubert, *Adv. Mater.* **2012**, *24*, 6397–6409.

[113] A. Vizintin, J. Bitenc, A. Kopac Lautar, K. Pirnat, J. Grdadolnik, J. Stare, A. Randon-Vitanova, R. Dominko, *Nat. Commun.* **2018**, *9*, 661.

[114] B. Pan, J. Huang, Z. Feng, L. Zeng, M. He, L. Zhang, J. T. Vaughey, M. J. Bedzyk, P. Fenter, Z. Zhang, A. K. Burrell, C. Liao, *Adv. Energy Mater.* **2016**, *6*, 1600140.

[115] Y. Xiu, Z. Li, V. Bhaghavathi Parambath, Z. Ding, L. Wang, A. Reupert, M. Fichtner, Z. Zhao-Karger, *Batteries & Supercaps* **2021**, *4*, 1850–1857.

[116] Z. Zhao-Karger, Y. Xiu, Z. Li, A. Reupert, T. Smok, M. Fichtner, *Nat. Commun.* **2022**, *13*, 3849.

[117] J. Bitenc, A. Scafuri, K. Pirnat, M. Lozinšek, I. Jerman, J. Grdadolnik, B. Fraisse, R. Berthelot, L. Stievano, R. Dominko, *Batteries & Supercaps* **2021**, *4*, 214–220.

[118] H. Dong, Y. Liang, O. Tutusaus, R. Mohtadi, Y. Zhang, F. Hao, Y. Yao, *Joule* **2019**, *3*, 782–793.

[119] S. Zhang, Y. Zhu, D. Wang, C. Li, Y. Han, Z. Shi, S. Feng, *Adv. Sci.* **2022**, *9*, e2200397.

[120] D. Bier, Z. Li, S. Klyatskaya, N. Sbei, A. Roy, S. Riedel, M. Fichtner, M. Ruben, Z. Zhao-Karger, *ChemSusChem* **2023**, *16*, e202300932.

[121] O. Lužanin, A. K. Lautar, T. Pavčnik, J. Bitenc, *Materials Advances* **2024**, *5*, 642–651.

[122] M. S. Chae, A. Nimkar, N. Shpigel, Y. Gofer, D. Aurbach, *ACS Energy Lett.* **2021**, *6*, 2659–2665.

[123] D. Monti, N. Patil, A. P. Black, D. Raptis, A. Mavrandonakis, G. E. Froudakis, I. Yousef, N. Goujon, D. Mecerreyes, R. Marcilla, A. Ponrouch, *ACS Appl. Energ. Mater.* **2023**, *6*, 7250–7257.

[124] B. Jiang, Y. Su, R. Liu, Z. Sun, D. Wu, *Small* **2022**, *18*, e2200049.

[125] M. Wang, C. Jiang, S. Zhang, X. Song, Y. Tang, H.-M. Cheng, *Nat. Chem.* **2018**, *10*, 667–672.

[126] a) S. Zhang, Y. L. Zhu, S. Ren, C. Li, X. B. Chen, Z. Li, Y. Han, Z. Shi, S. Feng, *J. Am. Chem. Soc.* **2023**, *145*, 17309–17320; b) C. Wang, R. Li, Y. Zhu, Y. Wang, Y. Lin, L. Zhong, H. Chen, Z. Tang, H. Li, F. Liu, C. Zhi, H. Lv, *Adv. Energy Mater.* **2023**, *14*, 2302495; c) F. Qiao, J. Wang, R. Yu, M. Huang, L. Zhang, W. Yang, H. Wang, J. Wu, L. Zhang, Y. Jiang, Q. An, *ACS Nano* **2023**, *17*, 23046–23056; d) C. Han, H. Li, Y. Li, J. Zhu, C. Zhi, *Nat. Commun.* **2021**, *12*, 2400.

[127] Z. Li, B. P. Vinayan, T. Diemant, R. J. Behm, M. Fichtner, Z. Zhao-Karger, *Small* **2020**, *16*, e2001806.

[128] K. A. See, J. A. Gerbec, Y.-S. Jun, F. Wudl, G. D. Stucky, R. Seshadri, *Adv. Energy Mater.* **2013**, *3*, 1056–1061.

[129] A. Scafuri, R. Berthelot, K. Pirnat, A. Vizintin, J. Bitenc, G. Aquilanti, D. Foix, R. Dedryvère, I. Arčon, R. Dominko, L. Stievano, *Chem. Mater.* **2020**, *32*, 8266–8275.

[130] Z. Zhao-Karger, R. Liu, W. Dai, Z. Li, T. Diemant, B. P. Vinayan, C. Bonatto Minella, X. Yu, A. Manthiram, R. J. Behm, M. Ruben, M. Fichtner, *ACS Energy Lett.* **2018**, *3*, 2005–2013.

[131] X. Yu, M. J. Boyer, G. S. Hwang, A. Manthiram, *Adv. Energy Mater.* **2019**, *9*.

[132] S. Wu, Z. Jiang, C. Wu, H. Li, J. Huang, N. Li, S. Huang, *Adv. Funct. Mater.* **2024**, *34*, 2313441.

[133] X. Zhou, J. Tian, J. Hu, C. Li, *Adv. Mater.* **2018**, *30*, 1704166.

[134] G. Bieker, J. Wellmann, M. Kolek, K. Jalkanen, M. Winter, P. Bieker, *Phys. Chem. Chem. Phys.* **2017**, *19*, 11152–11162.

[135] D. Zhou, X. Tang, X. Zhang, F. Zhang, J. Wu, F. Kang, B. Li, G. Wang, *Nano Lett.* **2021**, *21*, 3548–3556.

[136] R. Zhou, Z. Hou, Q. Liu, X. Du, J. Huang, B. Zhang, *Adv. Funct. Mater.* **2022**, *32*, 2200929.

[137] Z. Zhao-Karger, X.-M. Lin, C. Bonatto Minella, D. Wang, T. Diemant, R. J. Behm, M. Fichtner, *J. Power Sources* **2016**, *323*, 213–219.

[138] S. Kim, N. T. Hahn, T. T. Fister, N. J. Leon, X.-M. Lin, H. Park, P. Zapol, S. H. Lapidus, C. Liao, J. T. Vaughey, *Chem. Mater.* **2023**, *35*, 2363–2370.

[139] Q. Zou, Y. Sun, Z. Liang, W. Wang, Y. C. Lu, *Adv. Energy Mater.* **2021**, *11*, 2101552.

[140] T. Shiga, Y. Hase, Y. Kato, M. Inoue, K. Takechi, *Chem. Commun. (Camb.)* **2013**, *49*, 9152–9154.

[141] T. Shiga, Y. Kato, Y. Hase, *J. Mater. Chem. A* **2017**, *5*, 13212–13219.

[142] L. Ye, M. Liao, K. Zhang, M. Zheng, Y. Jiang, X. Cheng, C. Wang, Q. Xu, C. Tang, P. Li, Y. Wen, Y. Xu, X. Sun, P. Chen, H. Sun, Y. Gao, Y. Zhang, B. Wang, J. Lu, H. Zhou, Y. Wang, Y. Xia, X. Xu, H. Peng, *Nature* **2024**, *626*, 313–318.

[143] R. J. Staniewicz, *J. Electrochem. Soc.* **2019**, *127*, 782–789.

[144] A. Meitav, E. Peled, *Electrochim. Acta* **1988**, *33*, 1111–1121.

[145] S. Geng, X. Zhao, Q. Xu, B. Yuan, Y. Wang, M. Liao, L. Ye, S. Wang, Z. Ouyang, L. Wu, Y. Wang, C. Ma, X. Zhao, H. Sun, *Nat. Commun.* **2024**, *15*, 944.

[146] Q. Xu, S. Geng, B. Yuan, M. Liao, L. Ye, X. Zhao, Y. Wang, X. Zhang, S. Wang, Z. Qu, H. Miao, Z. Yang, Y. Gao, B. Wang, Y. Zhou, H. Peng, H. Sun, *Adv. Funct. Mater.* **2022**, *33*, 2210343.

[147] W. Ren, F. Xiong, Y. Fan, Y. Xiong, Z. Jian, *ACS Appl. Mater. Interfaces* **2020**, *12*, 10471–10478.

[148] a) J. Zou, J. Zhao, B. Wang, S. Chen, P. Chen, Q. Ran, L. Li, X. Wang, J. Yao, H. Li, J. Huang, X. Niu, L. Wang, *ACS Appl. Mater. Interfaces* **2020**, *12*, 44850–44857; b) M. Mao, Y. Tong, Q. Zhang, Y. S. Hu, H. Li, X. Huang, L. Chen, L. Gu, L. Suo, *Nano Lett.* **2020**, *20*, 6852–6858; c) Z. Meng, A. Reupert, Y. Tang, Z. Li, G. Karkera, L. Wang, A. Roy, T. Diemant, M. Fichtner, Z. Zhao-Karger, *ACS Appl. Mater. Interfaces* **2022**, *14*, 54616–54622.

[149] Y. Zhang, J. Xie, Y. Han, C. Li, *Adv. Funct. Mater.* **2015**, *25*, 7300–7308.

[150] T. Megyes, T. Grósz, T. Radnai, I. Bakó, G. Pálinkás, *J. Phys. Chem. A* **2004**, *108*, 7261–7271.

[151] K. Kisu, S. Kim, T. Shinohara, K. Zhao, A. Zuttel, S. I. Orimo, *Sci. Rep.* **2021**, *11*, 7563.

[152] L. H. B. Nguyen, J. S. Filhol, *Adv. Energy Mater.* **2023**, *13*, 2300311.

[153] Y. Zhong, C. Cao, L. Zhao, M. O. Tadé, Z. Shao, *Green Carbon* **2024**, *2*, 94–100.